IEEE Access
Multidisciplinary | Rapid Review | Open Access Journal

Received November 2, 2021, accepted November 13, 2021, date of publication November 16, 2021,
date of current version November 30, 2021.

Digital Object Identifier 10.1109/ACCESS.2021.3128774

A Study of Reduced Battery Degradation Through State-of-Charge Pre-Conditioning for Vehicle-to-Grid Operations

TRUONG M. N. BUI, MUHAMMAD SHEIKH, TRUONG Q. DINH, (Senior Member, IEEE), ANIRUDDHA GUPTA, DHAMMIKA W. WIDANALAGE, (Member, IEEE), AND JAMES MARCO
WMG, University of Warwick, Coventry CV4 7AL, U.K.

Corresponding author: Truong M. N. Bui (truong.bui@warwick.ac.uk)

This work was supported by Innovate UK through EV-elocity project 104250 and APC through eBSA project 75281.

ABSTRACT Transport electrification is a key enabler to reduce fossil fuel depletion and related carbon dioxide emissions. However, critical barriers exist in terms of battery costs and their expected life. Vehicle-to-grid technology can bring benefits to both the electrical power grid and electric vehicle owners, while its practical implementation faces challenges due to the concerns over accelerated battery degradation. This paper presents a comprehensive study on reduced Lithium-ion battery degradation through state-of-charge pre-conditioning strategies that allow an electric vehicle to participate in vehicle-to-grid operations during periods in which the vehicle is parked. Energy capacity reduction of the electric vehicle battery are predicted using semi-empirical ageing models, which have been built and validated to capture the degradation behaviours of the battery with respect to both calendar and cycling ageing. Five charging strategies for battery state-of-charge pre-conditioning have been developed to evaluate the ability to mitigate battery ageing before commencing vehicle-to-grid operations. Simulation studies on battery degradation utilizing such charging mechanisms under two different operational profiles have been undertaken. The analytical results show that the proposed charging strategies do not accelerate battery degradation and are capable of mitigating the total ageing process from 7.3 – 26.7% for the first 100 days of operational life and gradually vary to 8.6 – 12.3% for one-year continual operation compared to the reference standard charging approach.

INDEX TERMS Electric vehicles, vehicle-to-grid, battery degradation, Lithium-ion battery, SoC preconditioning, smart charge, semi-empirical model.

NOMENCLATURE

ABBREVIATION

BMS	Battery management system.
C	Charge/Discharge current rate.
CC	Constant current.
CC-CV	Constant current – constant voltage.
°C	Degree of Celsius.
CHA	Charge.
DCH	Discharge.
DoD	Depth-of-discharge.
EFC	Equivalent full cycle.
EoL	End-of-life.
EV	Electric vehicle.
GPR	Gaussian process regression.
MAE	Mean absolute error.
PDE	Partial differential equation.
RPT	Reference performance test.
SoC	State-of-charge.
SoH	State-of-health.
SC V1G	Battery charging following V1G method.
SC V2G	Battery charging following V2G method.
SC VxG	Battery charging with optimal SoC pre-conditioning method.
STD CHA	Standard charging method.
TS CHA	Time-shifted charging method.
V1G	Uni-directional power flow operation (battery charging without feeding their energy to the grid).

The associate editor coordinating the review of this manuscript and approving it for publication was Vitor Monteiro.

V2G Vehicle-to-Grid, Bi-directional power flow operation (battery charging with feeding their energy to the grid).

SYMBOLS AND VARIABLES

Ah	Ampere-hour.
$CalV1G$	Calendar ageing due to V1G.
$CalV2G$	Calendar ageing due to V2G.
C_p	Battery capacity.
$CycV1G$	Cycling ageing due to V1G.
$CycV2G$	Cycling ageing due to V2G.
Q_a	Calendar capacity loss at arrival SoC.
Q_{go}	Calendar capacity loss at global optimal SoC.
Q_{lo}	Calendar capacity loss at local optimal SoC.
$Q_{lossV1G}$	Capacity loss of V1G scenario.
$Q_{lossV2G}$	Capacity loss of V2G scenario.
Q_{loss}^{cal}	Calendar capacity loss.
Q_{loss}^{cyc}	Cycling capacity loss.
$Q_{loss}^{measured}$	Total measured capacity loss.
$Q_{loss}^{predicted}$	Total predicted capacity loss.
Q_{loss}^{total}	Total capacity loss.
SoC_{ar}	Arrival SoC.
SoC_{go}	Global optimal SoC.
SoC_{lo}	Local optimal SoC.
T_c	Battery charging time.
T_{in}	Battery connected time.
T_{out}	Battery disconnected time.
T_p	Parking time.
T_r	Battery resting time.
T_s	Charge starting time.
ΔCal	Absolute change of calendar ageing.
ΔCyc	Absolute change of cycling ageing.
ξ_T^{cal}	Calendar temperature coefficient.
$\tilde{\xi}_T^{cal}$	Calendar temperature coefficient curve.
ξ_T^{cyc}	Cycling temperature coefficient.
ξ_{SoC}^{cal}	Calendar SoC coefficient.
$\tilde{\xi}_{SoC}^{cal}$	Calendar SoC coefficient curve.
ξ_{DoD}^{cyc}	Cycling DoD coefficient.
ξ_{Crate}^{cyc}	Cycling C-rate coefficient.
γ^{cal}	Calendar exponential factor.
γ^{cyc}	Cycling exponential factor.

I. INTRODUCTION

The growth of electric vehicles (EVs) illustrates a small segment of the entire global automotive industry, but their market infiltration is significantly increasing due to their considerable benefits in dealing with environmental concerns. Vehicle-to-grid (V2G) technology, which allows the EV batteries to be connected to the power grid to provide energy and support ancillary services (e.g. frequency regulation, peak shaving and load levelling), is becoming increasingly important, especially where conventional forms of energy storage are unavailable or costly [1]–[5]. In V2G scenarios, the EV batteries are not only charged, but also can act as mobile energy storage systems to return energy back to the grid when the vehicle is parked and remains connected. A major challenge obstructing the implementation of V2G is the concerns over battery degradation, an unavoidable characteristic of the battery that happens in both operating and resting conditions [1]. When the battery is in a relaxing state, the capacity loss is considered as calendar ageing which represents the dependency of capacity fade to the resting or storing conditions and is independent of charge-throughput. Conversely, when the battery is electrically loaded, the capacity reduces which is recognised as cycling ageing, describing the influences of cycling conditions such as charging rates (C-rates), charge throughput, depth-of-discharge (DoD) and temperature of the battery. Theoretically, the battery life is declined when the number of charge cycles increases, hence, level and quantity of V2G operations should be calculated and optimised as accurately as possible to avoid excessive ageing through V2G operation [6]–[8]. Literature also shows that the degradation owing to calendar ageing can also be predominant over that of cycling ageing, especially when the magnitude of applied C-rates and DoD are low [9]–[11]. Thus, when capturing and evaluating the overall battery degradation in V2G operations, the degradation factors including the correlation of calendar and cycling ageing must be considered.

Number of studies focusing on the different methodologies to deal with battery degradation when participating in V2G can be found in the literature [12]–[15]. Amamra *et al.*, [14] presented an optimised bidirectional V2G operation based on a fleet of EVs connected to a distributed power system through a network of charging stations. The system could respond to the real-time EV usage data and identify the required changes for further optimising the use of EVs to support both frequency and voltage regulation with the consideration of minimising the battery degradation. Uddin *et al.*, [15] reviewed the associated technologies for better managing the battery usage in grid applications. The authors suggested an approach to extend battery life by formulating and solving an optimisation problem so that V2G could be effectively employed to control the EV resting condition and number of charge cycles to improve battery longevity. Yue Yu *et al.*, [16] presented a framework of optimal EV charging/discharge strategies for ancillary services of a smart grid by proposing a multi-objective optimisation task to minimise the system losses and battery cycling degradation. Marongiu *et al.*, [17] studied the effect of different V2G strategies on the lifetime of two different li-ion batteries types to show how the ageing effect of the batteries could be reduced. However, most of the studies focus on evaluating either calendar ageing or cycling ageing under fixed operational conditions. Only a few studies attempted to combine both ageing mechanisms into a single ageing model to evaluate the holistic battery degradation behavior [18], [19]. Nevertheless, the models we're not evaluated under real-world operational conditions.

TABLE 1. EV charging and battery degradation evaluation through V2G operations.

Ageing model approach	Charging approach	Source	Optimisation criteria	Benefits	Limitations
Averaged wear cost model	Standard charge	[12]	Battery wear cost	- Fast calculation - Predict for charge/ discharge cycles	- Calendar ageing ignored - Unable to accurately predicting cycling ageing
	Charge scheduling	[14]	Charge cost, Battery wear cost	- Easy to implement - Scheduling regulation up/ down	- Calendar ageing ignored - Based on averaged charge/ discharge rate - Fixed ageing rate
Linearized wear cost model	Standard charge	[13]	Battery wear cost	- Fast calculation - Energy throughput included	- No calendar ageing considered - Fixed ageing rate
	Flexible charging	[20]	Charge cost	- Control charge on peak demand - Perform peak shaving	- Calendar ageing ignored - Inaccurate wear cost
With advanced ageing model (Empirical, Semi-empirical, electrochemical, data-driven)	Charge scheduling	[16]	Charge cost, Battery wear cost	- Scheduling charging rate - Consider both calendar and cycling ageing	- Model complexity - Suitable for small-scale network
	Standard charge	[18]	SoC, DoD, temperature	- Multi-objectives optimisation - Consider both calendar and cycling ageing	- Current rate is ignored - Calendar ageing estimated twice
	Smart charge V2G	[19]	SoC, temperature, current	- Low calculation cost - Combined cycling and resting periods	- Model is accurate within a small operational range - Inaccurate at high DoD
	Smart charge V2G	[21]	Charge cost, SoC, battery wear cost	- Optimised charging process - Various charging architecture presented	- EVs on an aggregator can be uncontrolled - Calendar ageing ignored
	Smart charge V2G	[22]	Battery wear cost, SoC, DoD, C-rate	- Several schemes suggested - Ageing prediction through cycling process	- Calendar ageing ignored - No test with real-world profiles
	Smart charge V2G	[23]	Battery wear cost, DoD, temperature	- Understand the correlations between charge/discharge, DoD, ambient temperature	- Calendar ageing ignored - No test with real data
	Smart charge V2G	[24]	Battery wear cost, state-of-energy, SoH	- Time-controlled charging - Consider ambient temperature. Estimated ageing-dependent cost	- Simple battery ageing employed. Charging scenarios do not cover entire operational range
Without ageing model	Smart charge V2G	[20, 25]	Charge cost, SoC	- Flexible charge rate power - Charge priority at off-peak time, discharge at peak time	- Battery ageing ignored - Need knowledge to design fuzzy logic controller
		[26]	Charge cost	- Optimised charge cost and discharge profit	- Battery ageing ignored

Besides, different smart charge strategies which produce charging plans to minimise the charging cost and battery degradation during the period in which the EV is parking have been introduced [20]–[26]. Table 1 summarises the charging approaches for V2G scenarios with and without considering the battery degradation behaviour. A charge strategy without feeding the battery energy back to the grid (often described as smart charge V1G) regulates charging period and magnitude of the EV chargers so that the battery can be charged at optimal time and C-rates. Thus, it can help lower the cost of charging. A V2G strategy utilizing bidirectional chargers optimises the battery charging performance (like V1G) but also allows it to transfer the energy back to the grid whenever needed. Hence, a V2G approach can help minimize the charging cost and provide additional benefits via the energy exchange [14] and through reducing the calendar and cycling ageing rates which are assisting to extend the battery life [15].

In this paper, the evaluation and analysis of reduced battery degradation is conducted through various charging control strategies for state-of-charge (SoC) pre-conditioning of EV batteries allowing the vehicles participating in V2G scenarios during their parking period. Firstly, to predict the battery capacity fade characteristics due to calendar and cycling ageing, semi-empirical ageing models are developed. The parameters of the models are identified and verified using experimental data of long-term ageing tests under different laboratory conditions for both calendar and cycling ageing. A single lifetime ageing model is then constructed by combining the calendar and cycling ageing models to facilitate the prediction of total battery capacity loss under different EV operational profiles. The obtained models are utilized to evaluate the degradation behaviours of the EV battery before engaging V2G scenarios.

As summarised in Table 1, a number of publications show how new charging methods, such as smart charge V2G, may

accelerate battery degradation. In the main, these publications only consider ageing as a function of increased charge throughput. The primary contribution of this paper is a more holistic understanding of battery degradation that includes the combined impact of both calendar and cycling ageing during vehicle charging. Within the context of electric vehicle charging, the process of pre-conditioning the storage SoC of the vehicle's battery to mitigate degradation has not been reported before. Additional contributions include the development and real-world evaluation of five new battery SoC pre-conditioning strategies to minimize battery degradation and their integration within a diverse range of charging methods, ranging from standard charging, time-shifted charging and V2G operations.

The remainder of this paper is organised as follows: The development and validation of calendar, cycling and combined ageing models and their parametrisation are presented in Section II. Five charging strategies including conventional and smart charge approaches are developed followed by the simulation and comparative analysis are discussed in Section III. Extensive studies suggest and conclusion are finally reported in Section IV.

II. BATTERY DEGRADATION MODEL DEVELOPMENT

The rate of battery degradation is often governed by how the battery is stored and utilised, which is typically characterised by the so-called ageing stress factors including temperature, SoC, charge throughput, DoD and C-rate [15]. Literature shows that the causes of capacity fade can be categorized into two groups namely calendar ageing and cycling ageing, dependent on different ageing stress factors. Generally, calendar ageing is mostly affected by the storing temperature, SoC and time which represents how long the battery placed in the storage or in resting state; while the cycling ageing is typically influenced by ambient temperature, number of charge cycles or charge throughput, C-rate and DoD [27]. There are several approaches to estimate battery SoC, DoD, state-of-health (SoH), state-of-temperature (SoT) for advanced battery management and life-time prediction under different operational conditions [28], [29]. The critical advantage of these techniques is that they can offer improved performance prediction for battery state estimation and life-time prediction. However, the challenge of using such advanced tools is they can increase the computational costs and hence, it is difficult to execute in a long-term operation. If the aim is to run the model on-line as part of the battery or charger control systems, cycling ageing is a complex process, where advanced modelling approaches seem to have limited impact in improving the performance of the target model, especially for long-term prediction tasks while more computational resources are required [29], [30]. Therefore, it is necessary to have a simple but efficient approach for the battery degradation modelling and state estimation to increase the capability of working with complex control strategies over long-term periods of time.

Several studies have developed different tools for battery state estimation and degradation modelling such as empirical models [27], [31], semi-empirical models [32]–[37], electrochemical-based models [38]–[41], data-driven-based and machine learning models [11], [42], [43]. In such models, empirical and semi-empirical models were computationally less demanding, and easier to implement. However, due to having fixed equation forms, their prediction performance is largely dependent on the quality of the measured ageing data from which they are parameterized. In contrast, electrochemical-based models provided significant insights into the battery ageing process. Due to the complexity of their underpinning partial differential equations (PDE) employed, this kind of model suffers from a high computational cost and complex implementation. To address this challenge, reduced-order electrochemical models are often considered to simplify the model formulation [41]. Nonetheless, the calculation time is still high compared to other models and is not usually suitable for long-term execution or prediction. Data-driven based models performed well in predicting the underlying mapping of ageing and uncertainty of the capacity loss. However, the model parameters should be obtained using machine learning methods, e.g. Gaussian process regression (GPR), which increases the design effort [11]. Therefore, semi-empirical ageing models were considered as the most feasible solution for implementation [11], [44]–[47]. This type of models possesses considerable accuracy, good prediction ability, fast calculating efforts, and thus are suitable for long-term prediction and real-time applications. Wei *et al.*, [48] presented an energy-throughput-based approach for predicting the cycling ageing behaviour of the battery in multiphysics-constrained fast charging operation. The simulation results show that it can predict the cycling ageing behaviour well under different driving profiles. However, the prediction performance is restricted by an assumption that the battery can withstand a particular cumulative charge flow before reaching the end-of-life (EoL). This drawback could lower the prediction performance of the model when operating under real-world driving cycles. Naumann *et al.*, developed semi-empirical calendar [32] and cycling ageing [33] models to identify the ageing behaviour of a commercial lithium-ion battery. The model parameterisation was based on the experimental calendar and cycling ageing datasets. The simulation results illustrated good agreement between the model prediction and the measure of ageing data with the absolute model errors of the calendar capacity loss below 2.2% while those for the combined ageing was below 1%. However, the models' parameterisation was strongly dependent on the final values of the measured ageing data disregarding the ageing rate difference between the calendar and cycling ageing. So, the ultimate models did not represent the entire ageing behavior of the battery thus limiting their application. Particularly, the capacity loss due to calendar ageing part were excluded from the cycling ageing parameterisation while the calendar ageing rate was assumed unchanged during calendar and cycling periods. This assumption is known not to be true since the calendar and cycling ageing rates are usually varied

during the life of the battery. Li *et al.*, [34] established a semi-empirical ageing mechanism based on the C-rate and temperature to solely describe the cycling behaviour of the battery. The predicted ageing behaviour of the model was used to underpin an adaptive multistage constant current – constant voltage (M-CC-CV) charging strategy for EVs in different situations. Nevertheless, the model was not verified while the charge throughput was not considered in this study. Hence, the model accuracy could only guarantee within the tested operational conditions that did not correlate to the full operational range of the battery.

Since the purpose of developing the degradation models in this study is to evaluate battery ageing under V2G applications, simple degradation models that satisfy the model accuracy and computational effort are deemed to be adequate. It is because the underpinning degradation mechanisms requiring high-fidelity models are not considered here. Instead, a model with fast execution rate is necessary to simulate long-term degradation behaviours of the battery in the scale of months and years of operational life. Hence, the semi-empirical modelling approach is selected for this study. The following sections will describe how this approach is utilised to estimate the reduction in energy capacity due to calendar and cycling ageing effects. In order to support the development of the degradation models, the following assumptions are applied:

- For the calendar degradation model, the ageing stress factors include storage temperature, SoC and time. The SoC coefficient of the model at the storing temperature of 25°C and 100% SoC is equivalent to 1 and considered as the reference condition. The effect of ambient temperature is only evaluated within the range of 0 – 60°C.
- For the cycling degradation model, the ageing stress factors include temperature, C-rate for charge and discharge, DoD and energy throughput. The cycling ageing dataset used to train the model is solely dependent on the cycling ageing, which is independent on calendar ageing. The effects of ambient temperature are not considered outside the region of 0 – 25°C due to the restriction of historical ageing dataset. The effect of DoD on the capacity loss is unchanged when evaluating the C-rate coefficients at any specific condition due to the limited ageing dataset, which is discussed further in section II.C. The discharge current C-rates are limited within 0.3 – 2C covering the entire operational condition.

A. CELL SELECTION AND LONG-TERM AGEING TEST MATRICES

To understand the battery ageing behaviours and support model parameter identification and verification, long-term ageing tests of a batch of brand-new Lithium-ion Nickel Manganese Cobalt ($Ni_xMn_yCo_{1-x-y}$) oxide cathode and LiC_6 (graphite) anode cylindrical cells were conducted. The model code of the cells under tested is INR21700 M50 manufactured by LG Chem. with a nominal voltage of 3.63V and rated capacity of 5.00Ah. The lower and upper cut-off voltages recommended by the manufacturer are 2.5V and 4.2V respectively. The aim of this long-term ageing tests is to estimate the evolution of the capacity fade for different use-cases. As documented in [18], capacity fade of the batteries occurs during both operation when the battery is loaded by an external current (considered as cycling ageing) and in idle when the battery is placed in resting or relaxing condition without any current (known as calendar ageing). The batch of cells was divided into two groups, one group was for calendar ageing tests and the other one was for cycling ageing tests. In each condition, three cells were used to ensure the consistency of the results and to reduce the negative impact of cell-to-cell variations. Before conducting the ageing tests, all cells were pre-conditioned allowing their materials stabilisation and removing the remaining electrochemical interactions within the cells caused by the manufacturing process. Then, the cells were characterised for model parameterisation purposes following the procedures described in our previous works [49]–[51]. Hence, at the beginning of the ageing tests, the cell characteristics were known, and their SoH were normalized to 100%.

TABLE 2. Battery ageing test matrix for calendar ageing.

(a) Training data

SoC (%)	Storing temperature (^{0}C)			
	0	25	45	60
0	3 cells	3 cells	3 cells	3 cells
2	3 cells	3 cells	3 cells	3 cells
5	3 cells	3 cells	3 cells	3 cells
10	3 cells	3 cells	3 cells	3 cells
30	3 cells	3 cells	3 cells	3 cells
50	3 cells	3 cells	3 cells	3 cells
60	3 cells	3 cells	3 cells	3 cells
70	3 cells	3 cells	3 cells	3 cells
80	3 cells	3 cells	3 cells	3 cells
85	3 cells	3 cells	3 cells	3 cells
90	3 cells	3 cells	3 cells	3 cells
95	3 cells	3 cells	3 cells	3 cells
100	3 cells	3 cells	3 cells	3 cells

(b) Validating data

SoC (%)	Storing temperature (^{0}C)		
	15	35	55
20	3 cells	3 cells	3 cells
75	3 cells	3 cells	3 cells

1) CALENDAR AGEING TEST

Calendar ageing experiments were performed by storing the cells at different temperatures and SoCs. The complete set of test conditions is in Table 1. In this study, the total storage time of the cells is 57 weeks (equivalent to about 400 days). The calendar test matrix consists of two set of cells, one set employed for model parameterisation (training purposes) as shown in Table 2 (a) and the second, for model validation as depicted in Table 2 (b).

Before and during the ageing tests, capacity measurements were made at the specific time interval (equivalent to about 14 days) to generate a set of initial cell capacities

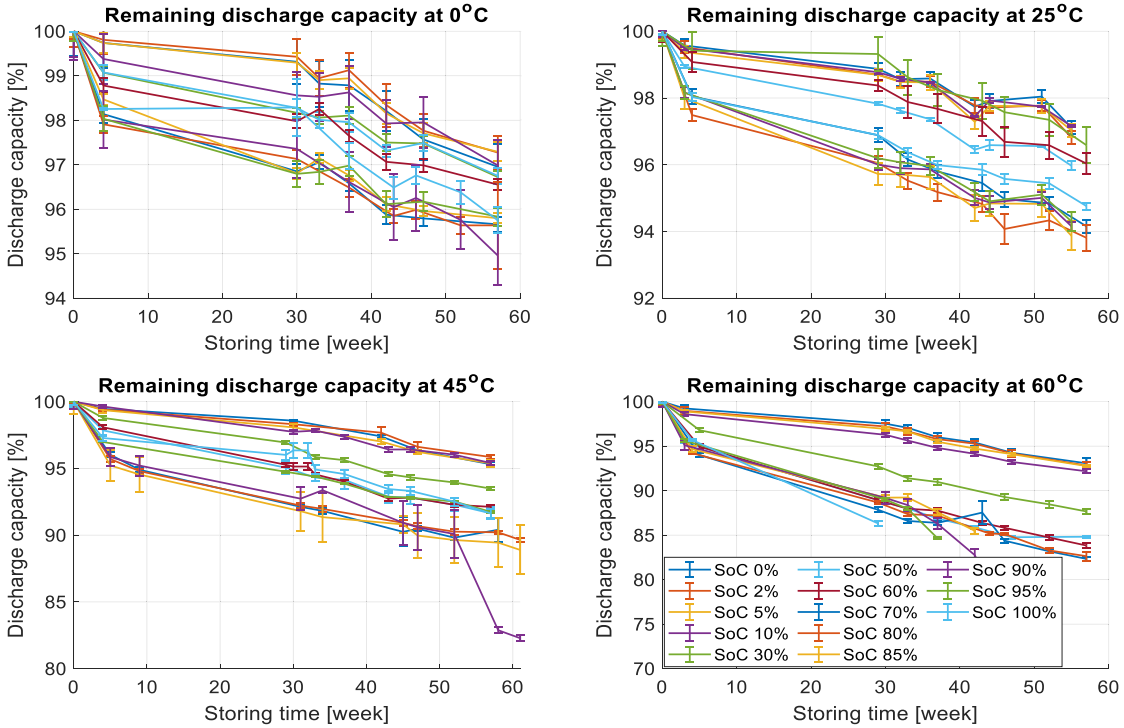

FIGURE 1. Remaining discharge capacity under calendar ageing at different storing temperatures.

and to quantify the calendar capacity loss of the cells. The capacity test was carried out using our reference performance test (RPT) protocol which is detailed in [52] and [53] and will therefore not be repeated here. For each storage temperature and SOC condition, three cells were employed to identify the mean and variation of capacity loss across the cells. The measured capacity loss of each cell was normalized against the initial capacity, then the final capacity loss of each test condition was calculated by averaging the normalized capacity. The capacity reductions versus storage time due calendar ageing are depicted in Figure 1. The reference capacity loss for calendar model parameterisation was selected from that of the test conditions (e.g., 100% SoC and at 25°C), which is highlighted in Table 1(a). Due to the restriction of laboratory access during the year 2020, capacity measurement tasks were unable to be performed during the time between week 4 and week 30. Hence, the capacity loss of this time was calculated by using a linear interpolation method based on the two adjacent measurements. The error bars associated to each measurement indicate the median and variance of the capacity loss of the cells for each ageing test.

2) CYCLING AGEING TEST

Cycling ageing tests were conducted by applying external current to charge (CHA) and discharge (DCH) the cells repeatedly at different C-rates and temperature conditions as depicted in Table 3. In these tests, the charging C-rates was limited at 0.3C as recommended by the manufacturer. The discharging current rates were varied at 0.3C, 1C and 2C,

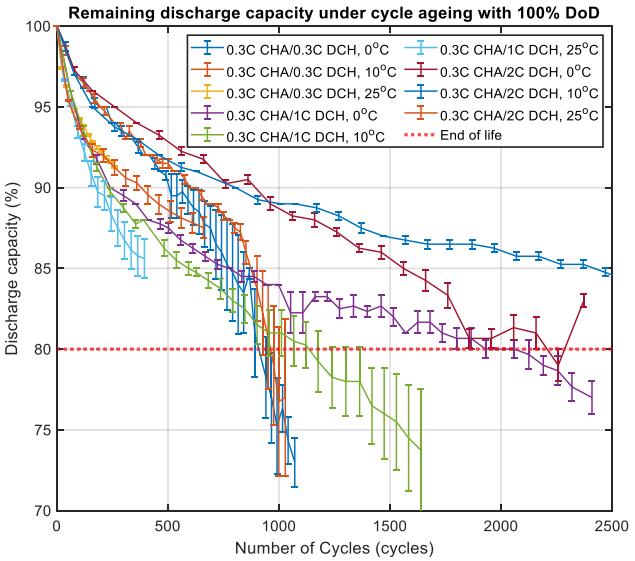

FIGURE 2. Battery discharge capacity under cycling ageing at different C-rates and temperatures.

respectively which cover the full range of operation at normal and peak load. The DoD of these cycling ageing tests was considered as of 100% of the cells were fully charged and discharged at desired C-rates and temperature.

Figure 2 presents the remaining cell capacity due to cycling ageing at different C-rates and temperatures. It is noteworthy that the desired temperatures in this study are restricted at 0°C, 10°C and 25°C due to the limitations of experimental

TABLE 3. Battery ageing test matrix for cycling ageing.

Temperature (^{0}C)	C-rates 0.3C CHA/ 0.3C DCH	0.3C CHA/ 1C DCH	0.3C CHA/ 2C DCH
0	3 cells	3 cells	3 cells
10	3 cells	3 cells	3 cells
25	3 cells	3 cells	3 cells

capability and local laboratory access, hence the temperature influence of the developing model is limited within such these bounds. Although the temperatures in these experiments do not cover the entire operating temperature of the battery, they are assumed to be representative of the target temperature of the model and valid for the current evaluation in this study.

Like the calendar ageing tests, three cells are employed for each experiment to capture the capacity reduction ensuring the consistency of the results. The error bars associated with each measurement indicate the median and variance of the capacity fade of the three cells for each test condition.

B. CALENDAR AGEING MODEL DEVELOPMENT

In this part, a semi-empirical calendar ageing model is developed to predict the effects of calendar ageing stress factors on the ageing behavior of the battery. The calendar ageing model is based on the Arrhenius equation which has been widely applied in the literature [11] to capture the capacity degradation during battery storage. The model parametrization is based on a complete calendar ageing dataset and overcomes the drawbacks of the model developed in [32] as mentioned in the previous section. Hence the model can predict the battery capacity reduction at any instant of storage time. In this model, the capacity loss due to calendar ageing is dependent on storage temperature, SoC and duration time t and can be expressed by the following equation:

$$Q_{loss}^{cal} = \xi_T^{cal}.\xi_{SoC}^{cal}.t^{\gamma_{cal}} \tag{1}$$

where, ξ_T^{cal} and ξ_{SoC}^{cal} are the calendar temperature coefficient and SoC coefficient, respectively; t is the storing duration, γ_{cal} is the calendar exponential factor ($\gamma_{cal} = 0.5$ [11], [32]).

1) CALENDAR TEMPERATURE COEFFICIENT

The calendar temperature coefficient represents the influence of store temperature to the capacity fade of the cell in the calendar ageing test. The calendar temperature coefficient can be described via the Arrhenius law as follows:

$$\xi_T^{cal} = \lambda_R.\exp\left(-\frac{\varepsilon}{R}\left(\frac{1}{T} - \frac{1}{T_R}\right)\right) \tag{2}$$

where, ε is the activation energy, R is the gas constant, T and T_R are the testing temperature and reference temperatures, λ_R is a reference constant which is calculated by the following term:

$$\lambda_R = \frac{Q_{loss}^{cal@25°C,100\%SoC,t}}{\xi_{SoC}^{R}.t^{\gamma_{cal}}} \tag{3}$$

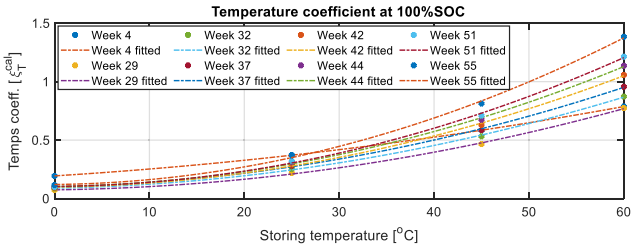

FIGURE 3. Calendar temperature coefficient fitted curves.

where, $Q_{loss}^{cal@25°C,100\%SoC,t}$ is the measured calendar capacity loss at the reference storing conditions, ξ_{SoC}^{R} is the reference SoC coefficient which is assumed to be equivalent to 1 for calendar ageing test at such reference storing conditions [24].

As a result, for each ageing snapshot measurement of different temperatures and SoC, a set of temperature coefficients can be calculated. A temperature coefficient curve can be then derived based on such set using a curve fitting method. These curves represent the influence of temperature on the calendar ageing over the whole operational temperature range, which is from 0 to 60°C in this study. Here, the temperature coefficients can be effectively represented by the following second order polynomial function:

$$\tilde{\xi}_T^{cal} = a_1T^2 + a_2T + a_3 \tag{4}$$

where, $\tilde{\xi}_T^{cal}$ is the temperature coefficient curve while a_1, a_2, and a_3 are the fitting coefficients of the polynomial.

A set of representative temperature coefficient curves at 100% of storing SoC is shown in Figure 3. To estimate the temperature coefficient at different storage temperature, SoC and storing time, a linear interpolation can be used. Meanwhile for estimating the coefficients beyond the temperature boundary, a linear extrapolation strategy could be employed based on the assumption that such coefficients are varied linearly outside the tested temperature conditions.

2) CALENDAR SoC COEFFICIENT

The SoC coefficient is calculated by transposing equation (1) into (5) as follows:

$$\xi_{SoC}^{cal} = \frac{Q_{loss}^{cal@T,SoC,t}}{\xi_T^{cal}.t^{\gamma_{cal}}} \tag{5}$$

where, ξ_{SoC}^{cal} is the SoC coefficient, ξ_T^{cal} is the temperature coefficient of any specific SoC and temperature that can be interpolated from equation (4).

Similarly, SoC coefficient curves, which represent the effects of SoC at different storing time, can be derived by linear curve fitting of the calculated SoC coefficients at each temperature and time. In this study, by using linear curve fitting approach, it has been found that the following third order polynomial expression could represent the SoC coefficient curves with the best fitness as follows:

$$\tilde{\xi}_{SoC}^{cal} = b_1SoC^3 + b_2SoC^2 + b_3SoC + b_4 \tag{6}$$

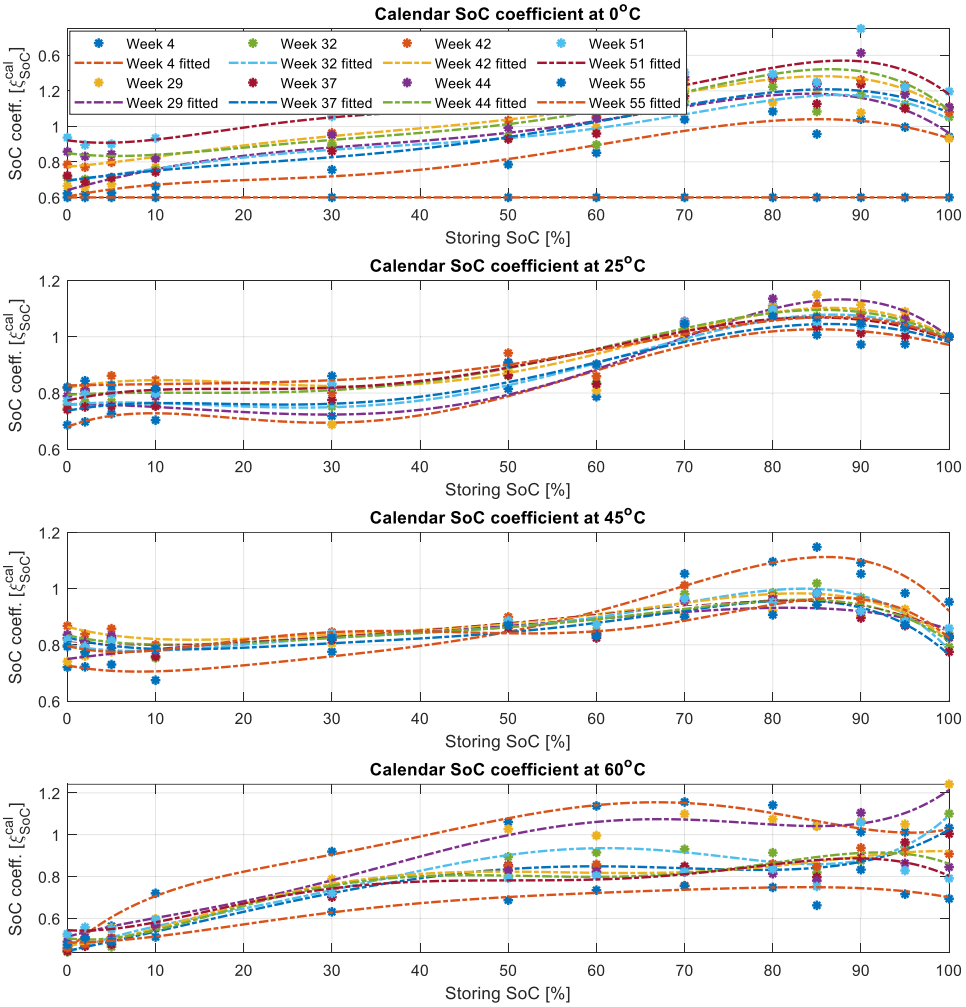

FIGURE 4. Calendar SOC coefficient curves at different temperatures.

where, $\tilde{\xi}_{SoC}^{cal}$ is the SoC coefficient curve, b_1, b_2, b_3, b_4 are the fitting coefficients of the polynomial.

The SoC coefficient curves, which describe the relationship between SoC coefficient and storage SoC, at different temperature and storing time are shown in Figure 4. To estimate the SoC coefficients at any storing SoC and any storing time, a linear interpolation method can be applied into two adjacent curves accordingly. Meanwhile, to estimate the SoC coefficients beyond the storing duration boundary given in Figure 1, a linear extrapolation approach could be applied whilst presuming such coefficients are changed linearly outside the tested period.

3) ACTIVATION ENERGY

The activation energy (ε) is calculated by taking the logarithm of both sides of equation (1) when the storage SoC is 100% at any temperature and time t, which is depicted as follows:

$$\ln\left(Q_{loss}^{cal@T,100\%SoC,t}\right) = -\frac{\varepsilon}{R}.\frac{1}{T} + \left(\frac{\varepsilon}{RT_R} - \ln\left(\xi_T^{cal}.t^{\gamma_{cal}}\right)\right) \tag{7}$$

By using first-order curve fitting method, equation (7) can be approximated as:

$$\ln\left(Q_{loss}^{cal@T,100\%SoC,t}\right) \cong \alpha\frac{1}{T} + \beta \tag{8}$$

where, $\alpha = -\frac{\varepsilon}{R}$ and $\beta = \frac{\varepsilon}{RT_R} - \ln\left(\xi_T^{cal}.t^{\gamma_{cal}}\right)$ are the fitting coefficients of the fitting function.

Finally, the activation energy can be calculated by evaluating the slope coefficient of the fitted curve (8) which is illustrated in equation (9).

$$\varepsilon = -\alpha.R \tag{9}$$

C. CYCLING AGEING MODEL DEVELOPMENT

In this section, a semi-imperial cycling ageing model is developed to predict the capacity reduction due to electrical loading of the battery. As mentioned, the cells were fully charged using constant current – constant voltage process (CC-CV) at 0.3C and fully discharged with constant current (CC) at three different current amplitudes, which are 0.3C, 1C and 2C, respectively. Because the cycling ageing tests were conducted repeatedly and continuously without any rest between two

adjacent cycles and only paused for capacity measurements every 14 days, it is assumed that the measured capacity drop dataset is purely due to cycling and independent on calendar ageing. This assumption means that the battery capacity fades due to calendar ageing can be neglected when evaluating cycling ageing results. The capacity loss due to cycling ageing is affected by the following stress-factors:

- Cycling temperature
- C-rates of charge and discharge cycle
- DoD or Charge bandwidth
- Charge throughput

In the cycling ageing experiments, the cells were fully charged and completely discharged using predefined constant currents. Hence, the DoD can be considered as 100% and unchanged during the tests. The general cycle ageing model can be presented as follows:

$$Q_{loss}^{cyc} = \xi_T^{cyc}.\xi_{Crate}^{cyc}.\xi_{DoD}^{cyc}.Ah^{\gamma_{cyc}} \tag{10}$$

where, ξ_T^{cyc}, ξ_{Crate}^{cyc}, ξ_{DoD}^{cyc} are the temperature coefficient, C-rates coefficient, and DoD coefficient, respectively. γ_{cyc} is the cycling exponential factor ($\gamma_{cyc} = 0.5$ [33]). Ah is the charge throughput or Ah throughput, which represents the amount of charge and discharge delivered by the battery during cycling, and can be expressed as follows:

$$Ah = EFC.DoD.C_P \tag{11}$$

where, EFC is number of equivalent full charge cycles and C_p is the battery capacity.

1) CYCLING TEMPERATURE COEFFICIENT

The operating temperature of the battery may significantly affect the performance of the battery and it is known that higher temperature may lead to increased degradation [24], [25]. Due to restricted historical data for modelling and testing, the measured cycling ageing data as shown in Figure 2 can be assumed as the target temperatures of the model and only valid for the current evaluation in this study. In fact, the battery temperature can always be controlled during the operation so that it can be maintained at either stable temperature or within small variation [45], [54]. Hence, the influence of temperature outside this region can be ignored. In this study, the operational temperature of the battery is assumed to be fully controlled and the temperature variation is small so that the temperature effects of the cycling ageing are supposed negligible. Consequently, the cycling temperature coefficient in equation (10) is equivalent to 1 [33]:

$$\xi_T^{cyc} = 1 \tag{12}$$

2) C-RATES COEFFICIENT

To parameterize the C-rates coefficient of the cycling ageing model, it is assumed that the influence of DoD on the capacity loss is unchanged and equivalent to 1 so that the relationship of total cycling capacity loss and charge throughput is linear. Consequently, the DoD coefficient will be re-estimated based on the calculated C-rates coefficient [33].

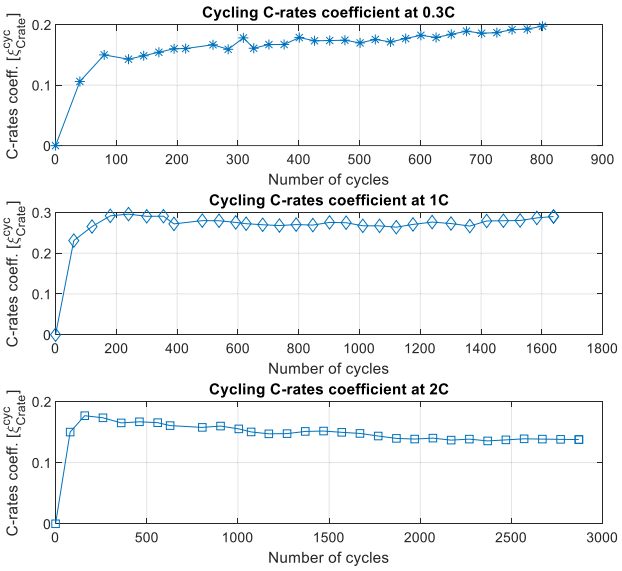

FIGURE 5. Cycling C-rates coefficients versus number of charge cycles.

$$\xi_{DoD}^{cyc} = 1 \tag{13}$$

By substituting (12) and (13) to (10), the influence of C-rates can be calculated as:

$$\xi_{Crate}^{cyc} = \frac{Q_{loss}^{cyc}}{Ah^{\gamma_{cyc}}} \tag{14}$$

The calculated C-rate coefficients versus number of charge cycles are depicted in Figure 5. To estimate the C-rate coefficients for either any specific EFC or C-rate within the region of 0.3C to 2C, linear interpolation was applied for the two adjacent coefficients.

3) DoD COEFFICIENT

Since the cycling ageing tests are only conducted with 100% of DoD, to calculate the DoD coefficient of the cycling ageing model, all test cases as shown in Table 2 are selected for the model training. The effect of temperature during cycling ageing is negligible, therefore the DoD coefficient can be calculated as follows:

$$\xi_{DoD}^{cyc} = \frac{Q_{loss}^{cyc}}{\xi_{Crate}^{cyc}.Ah^{\gamma_{cyc}}} \tag{15}$$

It can be seen that the estimated DoD coefficients, as shown in Figure 6, are varied depending on the number of EFC and C-rate. To estimate the DoD coefficient at either EFC or for any C-rate within the region of 0.3C to 2C, linear interpolation was applied for the two adjacent coefficients. Due to the lack of measured ageing datapoints at different DoDs, the calculated DoD coefficients are only valid if the DoD is 100%. Further tests are being undertaken out for extending the validity of the model for different DoD values.

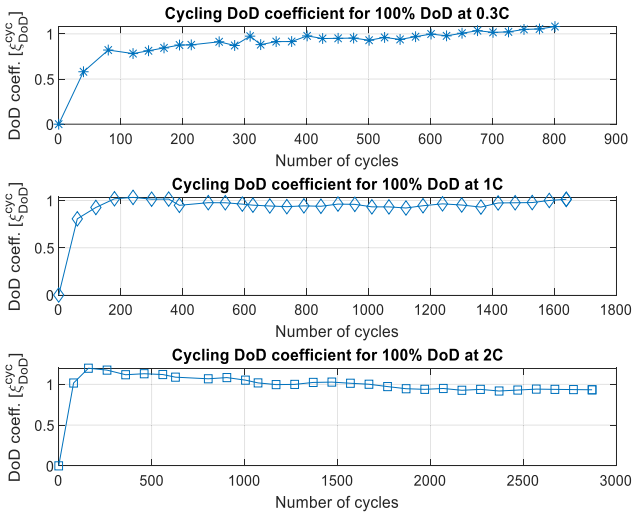

FIGURE 6. DoD coefficients versus number of charge cycles.

Finally, by substituting equations (11), (12), (14), and (15) into (10), the final energy capacity loss due to cycling ageing at any C-rate, DoD and Ah throughput can be estimated.

D. COMBINED CALENDAR AND CYCLING AGEING MODEL

Since the parameterization is based on the experimental calendar and cycling ageing datasets, the combination of calendar and cycling ageing can be presented as a simple summation of the calendar ageing model in equation (1) and the cycling ageing model in equation (10), resulting in the combined ageing model in equation (16) as follows:

$$\begin{aligned} Q_{loss}^{total} &= Q_{loss}^{cal} + Q_{loss}^{cyc} \\ &= \xi_T^{cal}.\xi_{SoC}^{cal}.t^{\gamma_{cal}} + \xi_T^{cyc}.\xi_{Crate}^{cyc}.\xi_{DoD}^{cyc}.Ah^{\gamma_{cyc}} \end{aligned} \quad (16)$$

Figure 7 shows schematically the combined degradation model framework. It is noteworthy that the total capacity loss can be calculated based on the combination of calendar and cycling ageing accordingly. This combination was considered in many studies in the literature as the basic approach for estimating the total battery ageing [18], [33], [55], [56]. To support the validation of this method, further work is being undertaken. The total capacity loss is dependent on the calendar ageing when the battery is in resting or relaxing state; while it is purely dependent on the cycling ageing when the battery is being electrically loaded. At any instant of time, either calendar or cycling ageing is considered as the main degradation mode to the total capacity loss.

E. AGEING MODELS VALIDATION

In this study, both ageing models are parameterized and validated from an experimental dataset that encompasses the envelope of operation for many real-world use-cases in terms of ambient temperatures and charge / discharge C-rates. Given the breadth and diversity of possible real-world driving and charging patterns it is not possible to represent all possible permeations within the training data for the models. However, it is noteworthy that the test-cycles employed for model validation are derived directly from real-world vehicle usage data, in particular commuter vehicle use within an urban environment. Validation against this data improves our understanding of model accuracy and the credibility of the model proposed. Additional research will be undertaken to widen the dataset employed for model validation by recording the behavior of different EV users considering variations in vehicle type, driver demographics and geographical location, to further refine the ageing models and their application to EV charging.

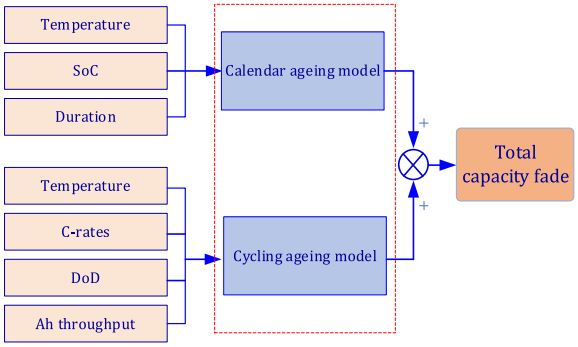

FIGURE 7. Combined degradation model framework.

1) CALENDAR AGEING MODEL VALIDATION

In this part, the developed calendar ageing model is validated using the historical data of the calendar ageing tests. The calendar ageing dataset for validation purposes are carried out along with those for training purposes; however, these capacity measurements are excluded from the model development and parametrization process. As shown in Table 1(b), the dataset for validation includes the measured calendar capacity loss versus storing time at three different storing temperatures (i.e., 15, 35 and 55°C) and two different storing SoCs (i.e., 20 and 75%). Figure 8 shows the comparison between the measured capacity loss and the predicted one using the developed calendar ageing model. In this step, a linear interpolation method is utilised to estimate the calendar SoC and temperature coefficients based on the two corresponding adjacent coefficients so that the calendar ageing model can predict the capacity drop for each snapshot measurement. Furthermore, the developed calendar ageing model employing the linear extrapolating algorithm can predict the calendar capacity loss at any storing condition beyond the tested one.

The prediction of calendar ageing performs well for the cases of 75% storing SoC since the predicted values are close or within the region of the error bar. As the result, the accuracy for this storing SoC condition is above 94% over the entire measured capacity loss while the mean absolute errors (MAE), as calculated using equation (17), are gradually increased from 0.084% (at 15°C) to 0.429% (at 55°C) owing to the increase of total capacity loss and storing temperatures. Conversely, due to the limited volume of training data at the

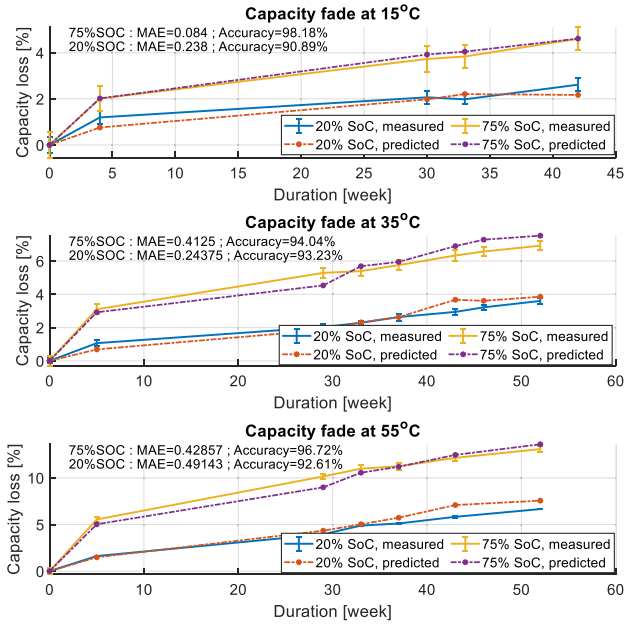

FIGURE 8. Calendar ageing model verification.

lower SoC regions during the model parameterisation, linear interpolation method does not give an accurate prediction for the cases of 20% storing SoC, hence the prediction accuracy is lower than that of the previous cases. However, the prediction results in this case are acceptable for further investigation within this study since the MAE are varied between 0.238% (at 15°C) and 0.491% (at 55°C). The prediction accuracy, which is the percentage between the MAE and the maximum measured capacity fade as calculated in equation (18), for these tests is above 90% over the entire capacity loss.

$$MAE = \frac{\sum_{i=1}^{n} \left| Q_{loss,i}^{measured} - Q_{loss,i}^{predicted} \right|}{n} \tag{17}$$

where, MAE is the mean absolute error, n is the number of measured data point, $Q_{loss,i}^{measured}$, $Q_{loss,i}^{predicted}$ are in turn the measured and predicted capacity loss, respectively.

$$Accuracy = \left(1 - \frac{MAE}{Q_{loss,\max}^{measured}}\right).100\% \tag{18}$$

where, *Accuracy* is the predicted accuracy, $Q_{loss,\max}^{measured}$ is the maximum measured capacity loss.

2) CYCLING AGEING MODEL VALIDATION

Due to the limited dataset of cycling ageing for training and validating the developed model, linear extrapolation method is employed to predict the cycling capacity loss by extending the known series of cycling ageing dataset gathered from the experimental cycling ageing tests. To perform the cycling ageing model validation, a ratio of training and testing data based on the series of the measured capacity loss of each discharge C-rates is generated. This ratio demonstrates the

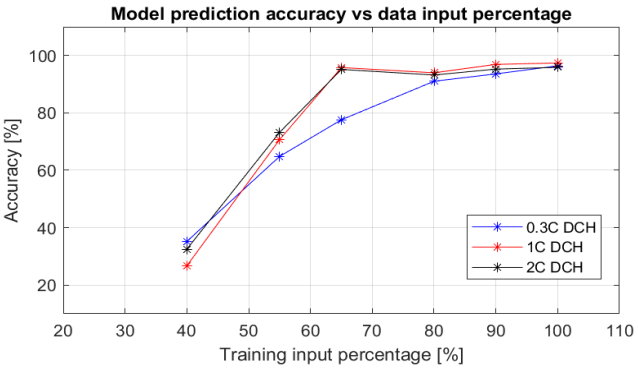

FIGURE 9. Prediction accuracy versus data input percentage.

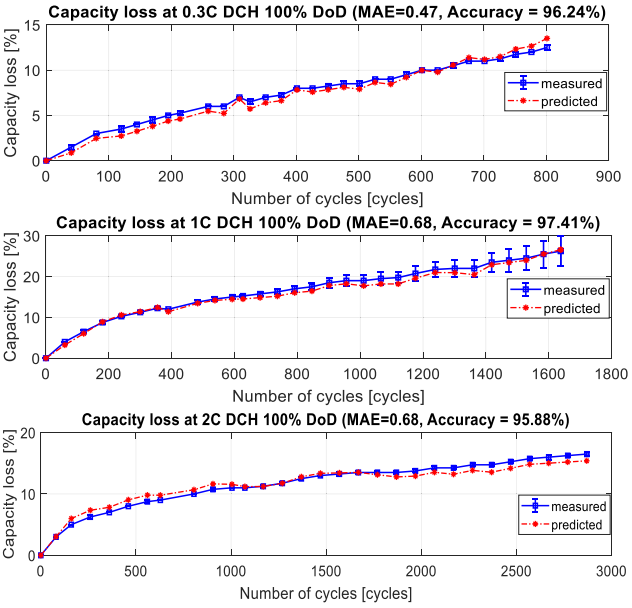

FIGURE 10. Cycling ageing model verification (with 100/0% input ratio).

number of measured ageing data being used for training versus the number of data being used for the validation purposes. Figure 9 shows the model prediction accuracy versus data input percentage of three different discharge rates (i.e., 0.3C, 1C and 2C) by starting with the ratio of 40/60% and gradually increasing this ratio data up to 100/0%.

From the figure, it can be seen that the more data being used for training, the better the prediction accuracy. At least 55% of measured data (for the cases of 55/45%) must be employed to obtain above 70% prediction accuracy of the model. As the best case, where 100% of historical ageing data is used for the training process, the prediction accuracy of the trained model can reach more than 95% over the entire measured capacity loss as depicted in Figure 10. Consequently, within the level of evaluating the developed models and charging control purposes for SoC pre-conditioning in V2G scenarios, the prediction accuracy of the developed models is sufficient and reliable for carrying on these works.

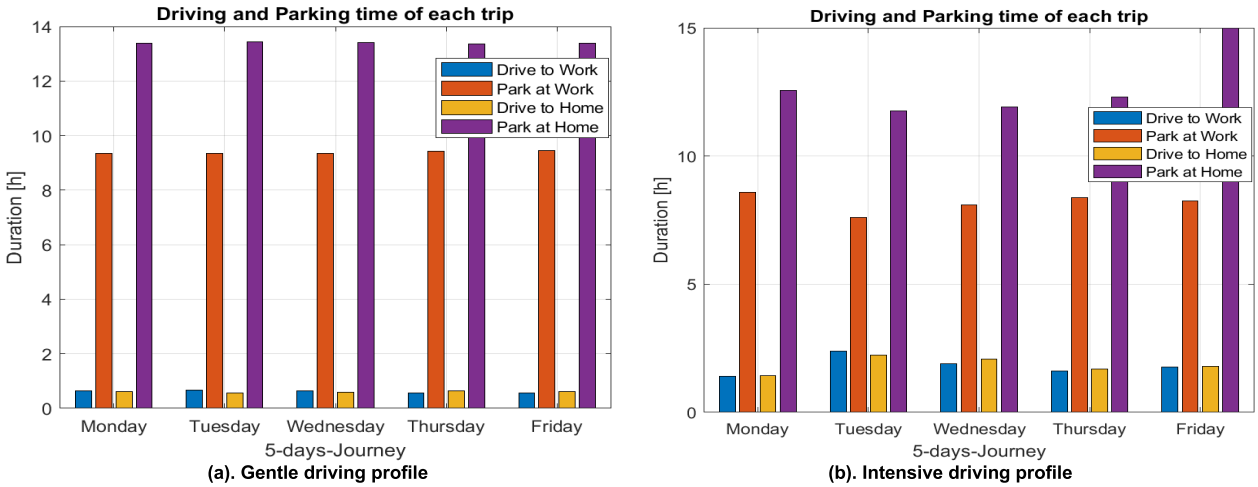

FIGURE 11. Two five-day operational profiles.

III. CHARGING STRATEGY DEVELOPMENT

In this section, five different SOC pre-conditioning charging strategies are proposed. The aim of these charging plans is to charge and/or discharge the battery to a predefined SoC level with less or minimal degradation before allowing the EV battery to participate in V2G operations. The developed charging strategies include standard charge (STD CHA), time-shifted charge (TS CHA), battery charging with SoC pre-conditioning using V1G (SC V1G), battery charging with SoC pre-conditioning using V2G approach (SC V2G), and battery charging with optimal SoC pre-conditioning (SC VxG). The detail of each strategy is explained in the following sections. The representative battery pack and its parameters employed in this study are shown in Table 4.

To evaluate the battery ageing behaviour under such charging strategies, two operational EV driver profiles are introduced based on the real data of EV driving trials and the customised parking, charging and stationary behaviors. The two operational energy driver profiles presented in Figure 11 are employed to represent the ''gentle'' or low energy demand driver and ''intensive'' or high energy demand driving profiles. Each profile lasts five days of operation (equivalent to 120 hovurs) representing a five-day journey. In these profiles, each operating day consists of two driving cycles (drive-to-work and drive-to-home) interspersed with two parking cycles (park-at-work and park-at-home) representing a complete daily operation of the EV. The mileage of each trip of the gentle profile is varied from 20 to 40 miles while those of the intensive profile is varied from 50 to 80 miles.

It is supposed that the EV owner will be leaving home and going to their work daily at 7:00am; upon arriving at the work car park, the driver connects the vehicle to the charger to fully charge the battery. Then at the end of the working day at 5:00pm, the owner unplugs the EV and returns home; upon arriving home, the owner once again plugs-in the vehicle to the charger so that the battery can be fully

TABLE 4. Representative battery information.

Parameters	Values	Units
Pack energy capacity	24	kWh
Pack nominal voltage	360	V
Pack configuration	100S13P	-
Cell capacity	5	Ah
Cell nominal voltage	3.63	V
V2G charger type	7	kW

charged for the next day. During parking at home and at the office's car park, the EV battery is allowed to participate V2G scenarios to exchange energy with the grid by using bi-directional V2G chargers. Figure 12 illustrates ten individual driving speed profiles obtained under each gentle and intensive driver styles and their corresponding SoC variation gathered from the real-world driver behavior for both gentle and intensive profiles. The vehicle battery is fully charged (100% SoC) at the beginning of each trip. The SoC at the end of each driving trip represents the SoC at the time of parking (arrival SoC). Hence, each sub-profile illustrates one driving trip of the complete five days operational profile, while the corresponding SoC is the actual battery drained of that trip.

It is noteworthy that each trip comprises of four individual operational modes which are driving, parking, charging, and resting. To facilitate the integration and evaluation of the battery ageing model in such operational profiles, it is assumed that the EV is correspondingly in the driving mode whenever it is driven (i.e., from home to work or vice versa). Upon arrival at the car park, the EV transitions to the park mode. Two short periods of time are added to the beginning and the end of parking mode simulating the driver plugging-in and unplugging the EV to/from the chargers. Then, the EV will take part in charging mode to fully charge the battery and the resting mode follows accordingly. It is noteworthy that the most important parameter of each daily trip is the arrival SoC, which indicates the starting SoC of the EV when it is connected to the charger. Hence, the impact of such driving

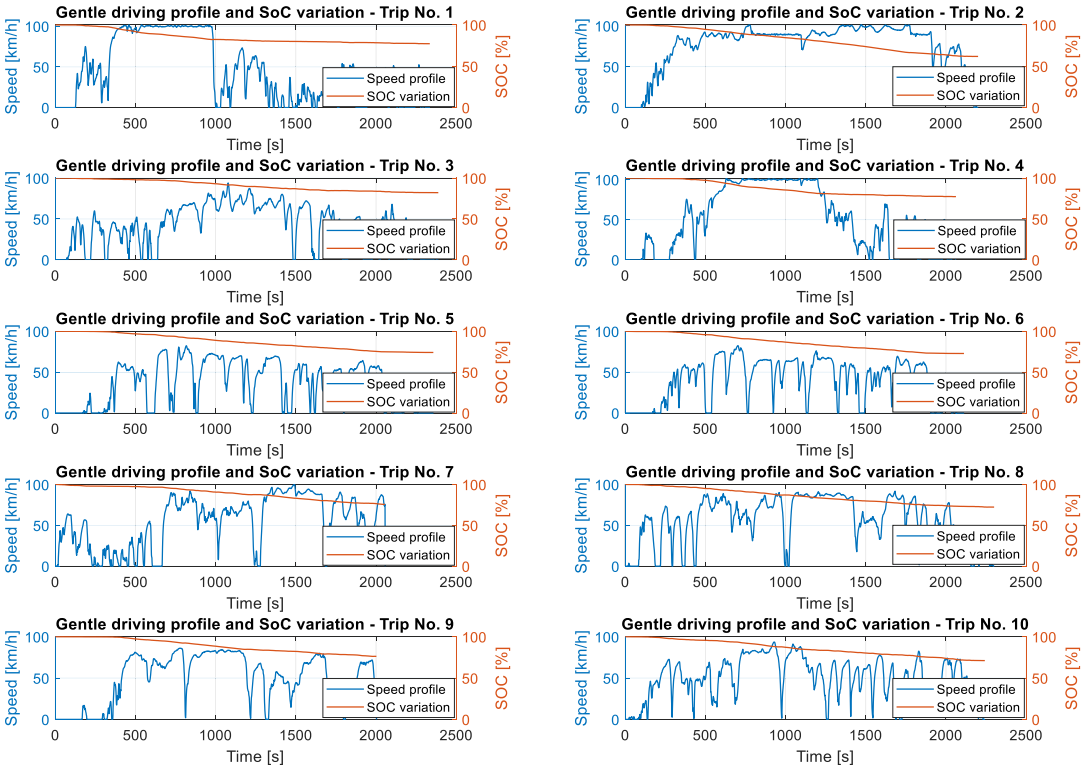

(a). Gentle driving profile

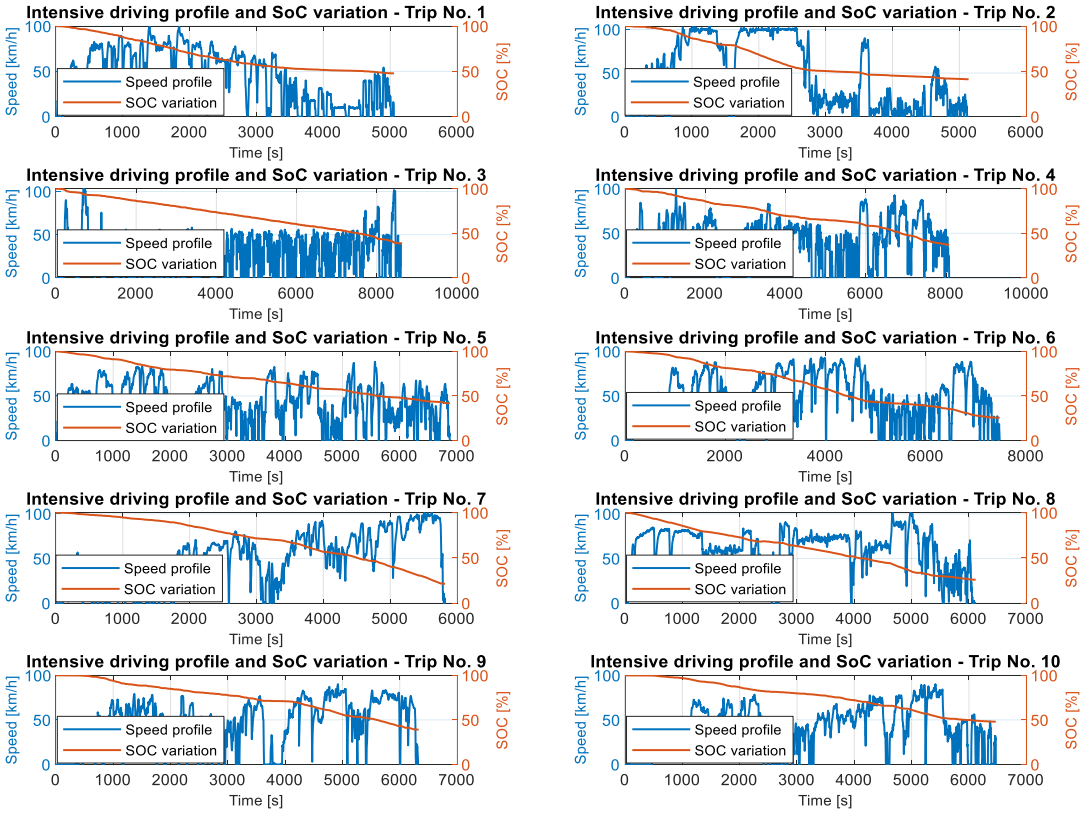

(b). Intensive driving profile

FIGURE 12. Individual driving trips and their SoC variation.

behaviours is not critical in this study, it just manifests itself as a change in SoC at the point of charging. The overview of five different SoC preconditioning schemes are described as follows:

- Standard charge strategy (STD CHA): is a conventional charging method. The EV battery is fully charged as soon as it is connected to the charger, leaving the EV in the rest state at 100%SoC until the next departure.
- Time-shifted charge strategy (TS CHA): is a smart charge method with a delayed charge time. The EV battery is rested at the point of parking and the instantaneous SoC is called the arrival SoC (or starting SoC). Based on the next departure schedule defined by the user, the battery charger is activated at an appropriate time so that the battery is fully charged just before the next departure time.
- Battery pre-conditioning using V1G (SC V1G): is a smart charge method without feeding energy back to the grid. By finding the lowest battery calendar ageing rate from starting the SoC to 100%, the charger drives the battery to the corresponding SoC level (hence named as local optimal SoC) before resting the battery. Based on the next departure schedule defined by the user, the battery charger is then activated at an appropriate time so that the battery is fully charged just before the next departure.
- Battery pre-conditioning using V2G (SC V2G): is a smart charge method with bidirectional energy flow back to the grid. The EV battery is only resting at the optimal SoC with the smallest calendar ageing rate over the whole SoC range (from 0% to 100%SoC, so called global optimal SoC). Here, the charger drives the battery to its optimal SoC by regulating the bi-directional energy flow between the battery and the grid. Based on the next departure schedule defined by the user, the battery charger is then activated at an appropriate time so that the battery is fully charged just before the next departure.
- Combined smart charge V1G and V2G (SC VxG): is the combination of SC V1G and SC V2G methods to trade-off between the absolute difference of calendar ageing (due to resting at optimal SoC) and the absolute difference of cycling ageing due to the addition of charge throughput (via bi-directional charging around the optimal SoC). Hence, at the beginning of each parking period, SC VxG strategy's controller selects the optimal charge/discharge for the battery to achieve the desired resting SOC condition that will minimise battery ageing.

Without loss of generality, it is assumed that the ambient temperature during both driving and parking periods is stable at 25°C. The whole simulation evaluation was carried out using a host computer workstation with an Intel Core i7-10850H 2.7GHz CPU, 32GB RAM within Matlab 2021a simulation environment. The sample time of the simulation and validation is fixed at 1 second. Detailed analysis of the complete five-day operational profiles with respect to the gentle and intensive energy drivers using the different charging strategies will be discussed in the following sections.

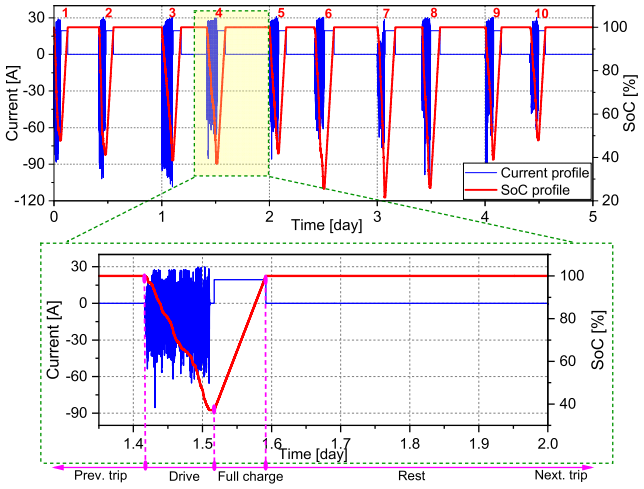

FIGURE 13. Intensive SoC operational profile with STD CHA strategy.

The main differences between the five charging schemes are summarised in Table 5.

A. STANDARD CHARGE STRATEGY

Conventional EV charging usually follows a nonlinear charging profile such as CC-CV [34]. However, to simplify the charging process in this paper, it is assumed that the battery is charged following constant current (CC) charge method to get the target SoC value. Therefore, in the STD CHA strategy, the EV battery will be fully charged with 0.3C rate representing the standard charging rate of the battery as soon as the battery is connected to the vehicle charger. Figure 13 illustrates the detail of the intensive driving profile with STD CHA strategy. As shown in the zoom-in subplot, the initial SoC at the beginning of each trip is always 100%, which means the battery is fully charged before each vehicle departure. Through driving, the battery is depleted to an end SoC representing the arrival SoC of the battery upon arrival of each trip. A delta SoC, which illustrates the amount of discharge the battery depleted through driving, can be calculated by evaluating the difference between the initial SoC and the end SoC. The EV is then plugged-in to the charger so that it can be fully charged for the next drive. As mentioned, the charge process will start immediately when the battery is connected to the charger. Consequently, upon being fully charged, the battery will be left in the resting mode until next departure. Similarly, the battery discharging, charging and resting period will be repeated accordingly for every following trip until the end of the operational profile. Ultimately, the intensive driving profile with STD CHA strategy is generated comprising ten individual trips which last for five days operation. In this figure, depending on the length of the driving profile, the time for driving, charging and resting period are different for each trip.

TABLE 5. Key characteristics of five charging strategies.

Strategies	Delayed charge time	Full charge start time	Resting SoC	Prior knowledge of parking period	Required bidirectional charger
STD CHA	No	When connected to the charger	100%	No	No
TS CHA	Yes	At an appropriate time before next departure	Arrival SoC	Yes	No
SC V1G	Yes	Preconditioning to a local optimal SoC, then full charge just before next departure	Arrival SoC or higher SoC with smaller calendar ageing rate	Yes	No
SC V2G	Yes	Preconditioning to a global optimal SoC for resting, then full charge just before next departure	Any SoC with least calendar ageing rate	Yes	Yes
SC VxG	Yes	Preconditioning to a global optimal SoC for resting, then full charge just before next departure	Any SoC with either least calendar ageing rate or having smaller cycling ageing rate (between SC V1G and SC V2G)	Yes	Yes

Figure 14 (a) presents the complete charging current and SoC profiles versus time of the gentle energy driver and their capacity loss prediction due to calendar and cycling ageing of the developed degradation models. Similarly, the current, SoC profiles and the ageing prediction of the intensive energy driver is shown in Figure 14 (b). To estimate the ageing behaviour of the battery over time, the capacity loss due to calendar ageing is only updated when the battery is in resting state. The same principle is applied for the cycling capacity loss, it is thus only updated when the battery is in driving or charging modes. Hence, during the first five days operational, the predicted capacity losses regarding to calendar and cycling ageing are gradually updated with respect to their stress-factors and the status of the battery. There is a large difference between the capacity loss of the battery on such two energy driver profiles. Table 6 shows the ageing results with respect to the gentle and intensive driving profiles with the STD CHA strategy for the first five days. The capacity losses due to calendar and cycling ageing are approximately at 0.0185% and 0.001% for the gentle profile and 0.0101% and 0.0105% for the intensive one, respectively. The cycling ageing in the gentle drive profile is much smaller than the calendar ageing because within this profile, the battery was being used very little and has spent more time in the resting state, especially when resting at high SoC level (100%). On the other hand, there is not much discrepancy between the calendar and cycling aging in the intensive driving profile. It is because the battery in this case has been used a lot for driving, which increase the charge throughput, and hence, increasing the cycling ageing while reducing the resting period. It also presents that the calendar aging is significant for gentle use, particularly resting at higher SoC level could have negative impact to the battery as it increases the calendar ageing. The total capacity fade predictions are 0.0195% and 0.0206% for these profiles. The results show that the employed charging strategy and the developed ageing models are effective in controlling the charging process and predicting the battery degradation over time. The battery aging results of the STD CHA strategy will then be used as the baseline reference for the comparative study with other charging strategies in this section.

TABLE 6. Battery ageing results with STD CHA strategy for the first five-day operation.

Strategy	Profile	Rest time (h)	No. of Cycles	Calendar (%)	Cycle (%)	Total (%)
STD CHA	Gentle	106.5	2.7	0.0185	0.001	0.0195
	Intensive	83.6	6.8	0.0101	0.0105	0.0206

B. TIME-SHIFTED CHARGE STRATEGY

Time-shifted charge (TS CHA) is developed to delay the charging process to the later time so that the capacity fade due to calendar ageing can be reduced. Different from STD CHA, where the battery is fully charged as soon as it is connected to the charger, The TS CHA method shifts the charging start time to an appropriate time while the battery is left in resting state at the SoC upon arriving (arrival SoC). In this strategy, the electrical tariff is supposedly unchanged during the test, a control algorithm will calculate suitable charging start time ensuring the battery will be fully charged just before the next departure. A prediction capability is therefore assumed between the driver, vehicle and charger in which the charging process starts to ensure that vehicle battery is fully charged just before the vehicle is needed.

Figure 15 presents the details of the intensive driving profile with TS CHA. In the zoom-in subplot, the initial SoC of each trip is always at 100%, which means the battery is fully charged at the beginning of the trip. Then, the battery is gradually discharged as it is in driving mode. Upon arrival at the car park and connection to the charger, the battery keeps holding at the arrival SoC. The charger controller calculates the amount of charge needed to fully charge the battery and estimates the necessary charging time based on the current SoC. Depending on the pre-set leaving time, the controller determines the appropriate start time to charge the battery. As a result, the five days operational profile of intensive energy driver with TS CHA is generated as shown in the top subplot.

Figure 16 (a) shows the operational current and SoC profiles over time of the gentle driving profile and their predicted calendar and cycling capacity losses while (b) depicts those

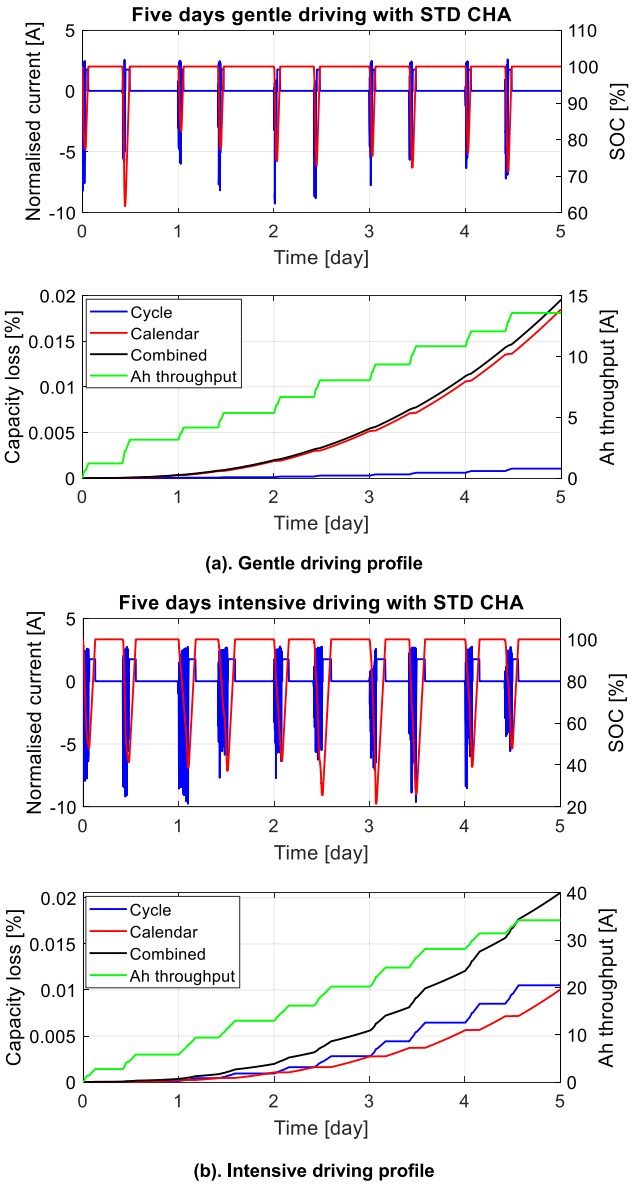

FIGURE 14. Prediction of battery ageing using STD CHA.

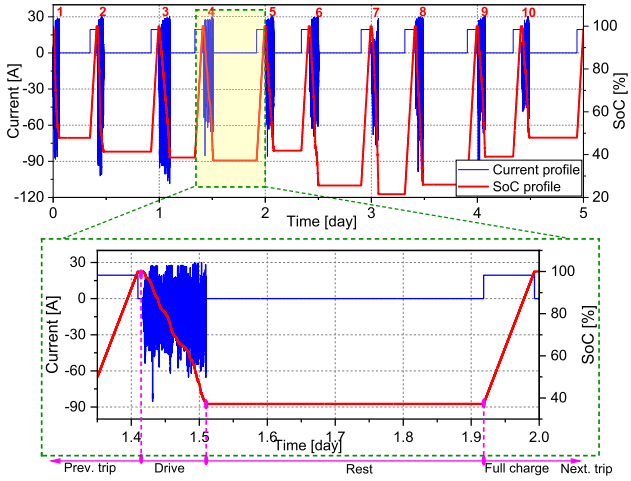

FIGURE 15. Intensive SoC operational profile with TS CHA strategy.

TABLE 7. Battery ageing results with TS CHA strategy for the first five-day operation.

Strategy	Profile	Rest time (h)	No. of Cycles	Calendar (%)	Cycle (%)	Total (%)
TS CHA	Gentle	106.5	2.7	0.0191	0.001	0.0201
	Intensive	83.6	6.8	0.0039	0.0105	0.0144

of the intensive energy driver profiles using the TS CHA strategy. Comparing to the baseline STD CHA, the total resting duration and number of charge cycles of TS CHA are unchanged. However, for this battery characteristic, TS CHA strategy provides better calendar ageing rate because it allows the battery resting at a lower SoC, which causes slower calendar capacity fade than that of resting at fully charged. This result is consistent with the historical ageing dataset in Figure 2 and the studies reported in the literature [11], [57]. Similar to the results of the gentle profile of the baseline strategy, the cycling ageing is much smaller than the calendar ageing because within this profile, the battery was being used very little and has spent more time in the resting state. However, due to having resting at lower SoC levels in the intensive driving profile, the calendar ageing in this case is significant reduced (0.0101% to 0.0039%, equivalent to 68% mitigation) comparing to the baseline. Table 7 summarises the battery ageing results of the two energy driver profiles with TS CHA approach for the first five days operation. The total capacity loss under the gentle driving profile is 0.0201% while that of the system under intensive driving profile is 0.0144%. Although the total capacity loss reducing of the gentle driving profile does not show any benefit, those of the intensive driving profile are significantly mitigated up to approximately 30% within the first five days operation as comparing to the baseline STD CHA strategy.

C. SC V1G STRATEGY

Battery SoC pre-conditioning using V1G (SC V1G) is developed based on the charging principles of the TS CHA strategy, considering the availability of a local optimal SoC (from arrival SoC to 100%) having a smaller value of calendar ageing than resting the battery as in TS CHA. SC V1G allows the charger to control both charging start time and SoC so that the battery calendar degradation rate can be maintained at a lower value than or equal to that of the arrival SoC. The control logic of this strategy can calculate the battery calendar ageing rates of the battery at different SoC levels (from the arrival SoC to 100% SoC) using the historical calendar ageing data. Based on this calculation, a local optimal SoC which offers the smallest calendar ageing rate can be identified. The charger will drive the battery SoC to that optimal level before taking rest for the rest of the parking duration.

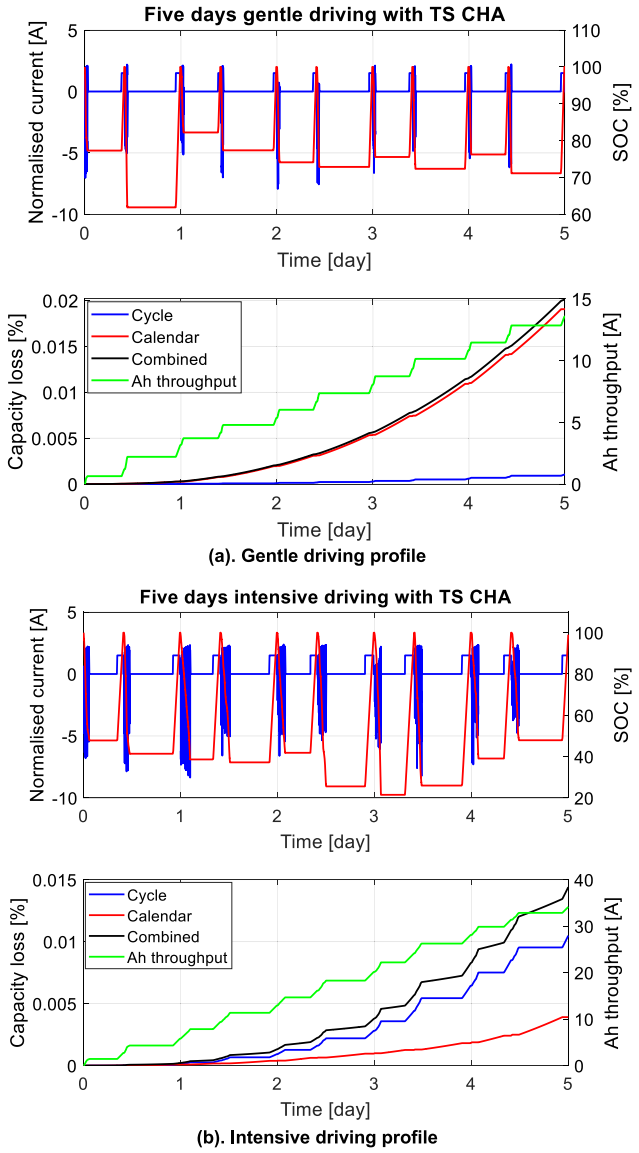

FIGURE 16. Prediction of battery ageing using TS CHA.

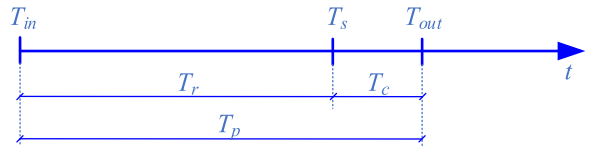

FIGURE 17. Timing constraints of the EV when parking.

The timing constraints of the EV battery when parking is shown in Figure 17. In this diagram, assuming the EV battery is connected to the charger at time T_{in} and will leave at time T_{out}, which indicate the arrival and departure time, respectively. The control algorithm calculates the full-charge time (denoted by T_c), which is the time required to fully charge the battery, based on the current SoC, the power capability of the charger or the remaining energy of the battery upon arrival. Then, the controller determines the charge start time

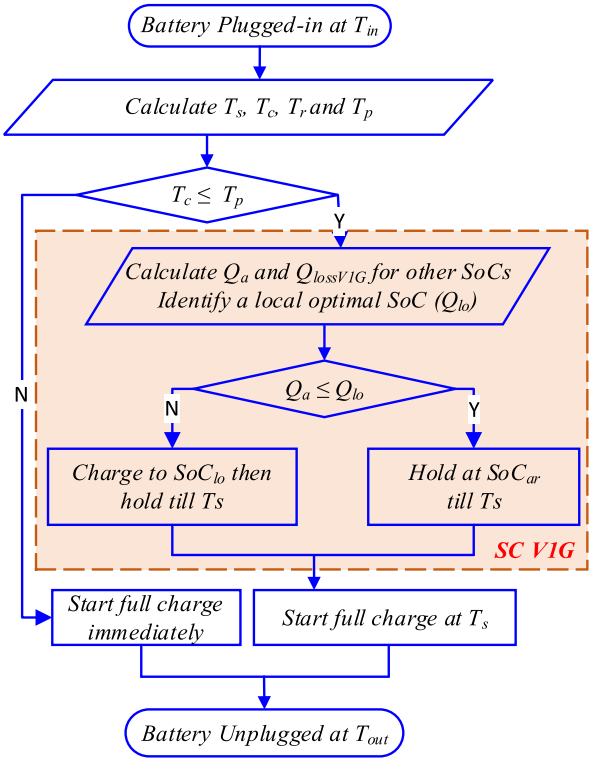

FIGURE 18. Smart battery pre-conditioning using SC V1G strategy.

(denoted by T_s), which is the time to begin to charge the battery, according to T_c. The term $T_p = T_r + T_c$ indicates the total parking time, which includes charging and resting time. Hence, if the full-charge time (T_c) is larger than or equal to total parking time (T_p), then the charger will perform a full charge promptly without the resting period. The following steps describe the control procedure of the SC V1G.

- Step 1: The controller estimates the increment of the calendar capacity loss if the battery is resting at the arrival SoC (SoC_{ar}) for a time of T_r, denoted by Q_a.
- Step 2: The controller estimates the increment of the calendar capacity loss if it is resting at any SoC level (from the arrival SoC to 100% SoC) for the time of T_r, denoted by $Q_{lossV1G}$.
- Step 3: From all possible $Q_{lossV1G}$, the algorithm identifies a local optimal SoC (SoC_{lo}), which is the SoC level (from the arrival SoC to 100%) with smallest calendar ageing denoted by Q_{lo}.
- Step 4: By comparing Q_a and Q_{lo}, the control algorithm can determine whether to hold the battery at SoC_{ar} until T_s or charging the battery to the SoC_{lo} then holding until T_s.

As soon as it is connected to the charger, the battery will be either held at the current SoC if the ageing rate of the arrival SoC is smaller than that of the local optimal SoC or charged to the local optimal SoC level, hence the battery maintains its charge capacity at lower calendar degradation rate during resting. The departure time must be pre-defined before participating this charging method.

TABLE 8. Order of calendar ageing rate with respect to SoC (low to high) for the first 28 days of storing.

	Order of calendar ageing rate with respect to SoC (1: low, 20: high)																			
	1	2	3	4	5	6	7	8	9	10	11	12	13	14	15	16	17	18	19	20
SoC (%)	30	25	20	35	5	15	10	40	45	50	55	60	65	70	100	75	95	80	90	85

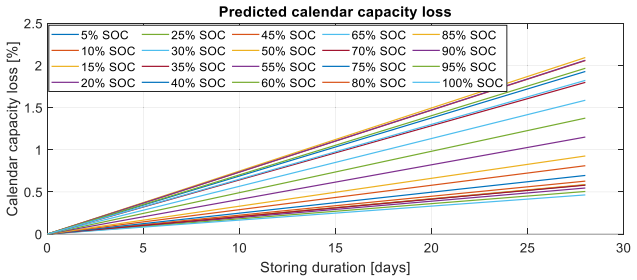

FIGURE 19. Calendar ageing rate with respect to SoC and storing duration of the first 28 days.

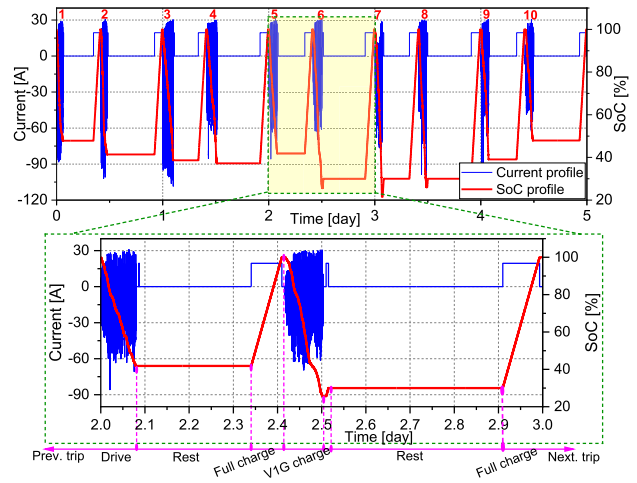

FIGURE 20. Intensive SoC operational profile with SC V1G.

The local optimal SoC can be extracted based on the historical data of the calendar ageing test. Figure 19 illustrates the interpolated SoCs at which the calendar aging rate changes for the first 28 days of storage. The order of SoCs from low to high is depicted in Table 8. Within the first 28 days, the SoCs having the least and the most calendar ageing rate are 30% and 85%, respectively.

Figure 20 shows the complete battery operational SoC profile of the intensive driving use case with SC V1G. The battery arrival SoC of any trips smaller than 30% (trip number 6, 7 and 8) will be charged up to 30% SoC, then remain unchanged at this charge during the rest period. It is because the local optimal SoC is 30% at this instant while any SoC levels lower or higher than 30% causes higher calendar ageing. Hence, based on the Figure 19, in the remaining trips (trip 1, 2, 3, 4, 5, 9 and 10), the battery is turned into resting mode right away at the arrival SoC.

The top subplots of Figure 21 (a) and (b) present the charging current and SoC profiles versus time of the gentle and intensive driving profiles while the bottom subplots show the predicted calendar and cycling capacity fade when using the SC V1G strategy accordingly for such two driving profiles. Table 9 depicts the summary of battery ageing results for the first five days operation. Comparing to the baseline STD CHA, the total calendar duration and number of charge cycles of the SC V1G are also unchanged. However, by allowing the battery to rest at a local optimal SoC, the calendar capacity losses are negligibly reduced in the gentle profile but significantly mitigated in the intensive profile (from 0.0101% to 0.0039%, equivalent to 61% reducing). The cycling ageing of both profiles is almost unchanged in this case due to having the same charge throughput with the baseline. Obviously, the SC V1G shows advantages when applying to the intensive driving profile, which has lower arrival SoC levels in most of the trips, whilst it is inexplicit in the gentle profile because resting at the arrival SoC in this case causes faster calendar ageing than having rested at fully charged. However, it is noteworthy that the calendar capacity loss could be significantly decreased if employed for more intensive driving profiles, particularly when the arrival SoCs are smaller than the local optimal SoC or at a different moment during the lifetime of the battery at which the local optimal SoC are always higher than most of the arrival SoC. Comparing to the baseline, there is no change in the total ageing for the gentle driving profile, but the total ageing improvement is notable for the intensive driving one as it reduces 30% of capacity loss.

TABLE 9. Battery ageing results with SC V1G strategy for the first five-day operation.

Strategy	Profile	Rest time (h)	No. of Cycles	Calendar (%)	Cycle (%)	Total (%)
SC V1G	Gentle	106.5	2.7	0.0185	0.001	0.0195
	Intensive	83.6	6.8	0.0039	0.0105	0.0144

D. SC V2G STRATEGY

Battery SoC pre-conditioning using V2G strategy (SC V2G) is developed based on the improvement seen in SC V1G strategy in term of charging and discharging capability. In this strategy EV batteries are allowed to discharge their energy to the grid whenever the arrival SoC is higher than the instant global optimal SoC disregarding the increment of charge throughput. A bidirectional V2G chargers with capability to charge and discharge the battery to the grid is required for this strategy. The timing constraints of the EV when parking is the same as those of the SC V1G. However, when doing SC V2G, the following steps are applied:

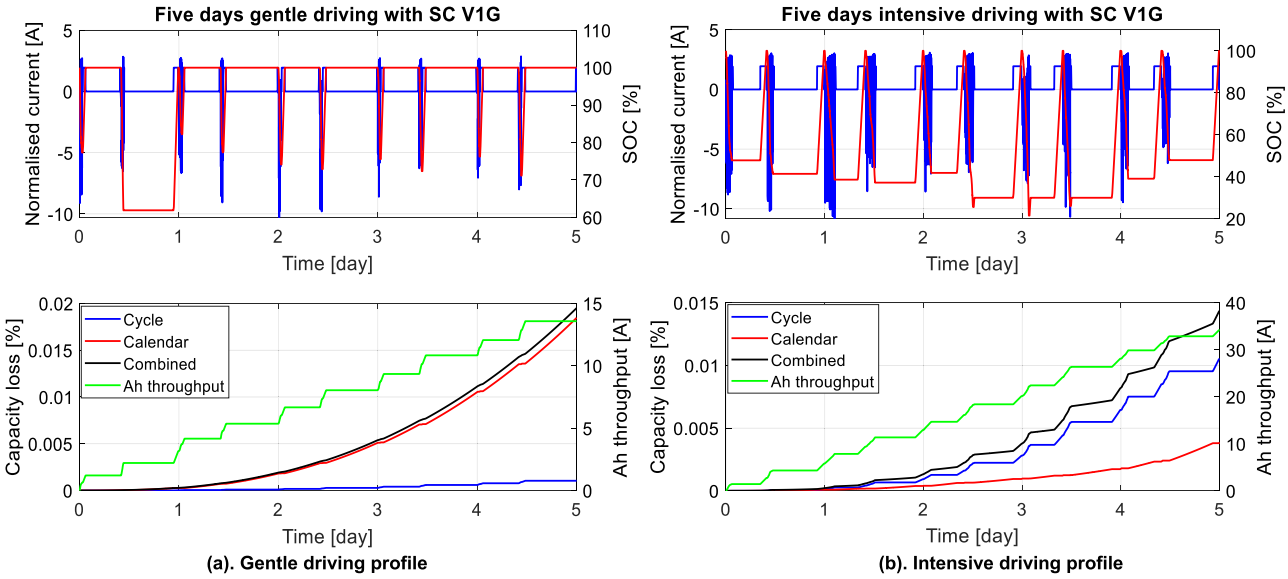

FIGURE 21. Prediction of battery ageing using SC V1G.

- Step 1: The controller estimates the increment of the calendar capacity loss (Q_a) when resting at the arrival SoC (SoC_{ar}) for the duration of T_r.
- Step 2: The controller estimates the calendar capacity loss when resting at any SoC level (from 0% to 100% SoC) for the time of T_r, denoted by $Q_{lossV2G}$.
- Step 3: From such $Q_{lossV2G}$, the algorithm can identify the global optimal SoC (SoC_{go}), which is the SoC level with the least calendar ageing, denoted by Q_{go}.
- Step 4: By comparing Q_a versus Q_{go} and SoC_{ar} versus SoC_{go}, the control algorithm determines whether to either hold the battery at SoC_{ar} until T_s or charge/discharging the battery to the SoC_{go} and then hold until T_s.

A diagram of this strategy is shown in Figure 22. SoC at 30% is also considered as the global optimal SoC (SoC_{go}) as seen in Table 8 because it has the least calendar ageing. Figure 23 presents the complete SoC operational profile of the intensive driving profile with SC V2G strategy for the first five days operation. The batteries of the trip number 1∼5, 9 and 10 are discharged to 30%, which is the SoC_{go}, while the batteries of trip number 6∼8 are charged up to SoC_{go} before resting for the duration of the park period. Comparing to previous charging strategies, the total resting duration of the SC V2G is consequently reduced due to having shorter resting time. Thus, the calendar capacity loss is significantly reduced. However, this strategy increases the total charge throughput, represented by the number of charge cycles. Theoretically, this behaviour is therefore causing some increment of cycling ageing. Especially, for the gentle driver profile, where the arrival SoCs are far from the global optimal SoC for this battery type.

Similar to the previous case-studies, Figure 24 (a) and (b) depicts the charging current and SoC profiles over time in the top subplots while the bottom subplots show the predicted

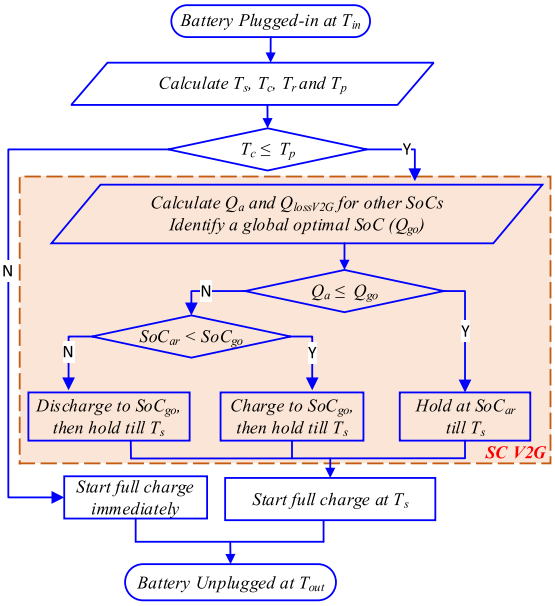

FIGURE 22. Smart battery pre-conditioning using V2G strategy.

calendar and cycling capacity fade variation using SC V2G strategy for the two energy driver profiles. Table 10 shows the battery ageing results of the first five-day of operation. Comparing to the baseline, the SC V2G calendar capacity loss is significantly reduced in both driving profiles (i.e., from 0.0185% to 0.0023% (equivalent to 88%) for the gentle driving profile; and from 0.0039% to 0.0025% (equivalent to 34%) for the intensive driving profile. This is because the resting time of the battery with SC V2G is significantly reduced due to increasing the charge throughput to reach to the global optimal point. The cycling ageing is also significantly increased in both profiles, which are equivalent

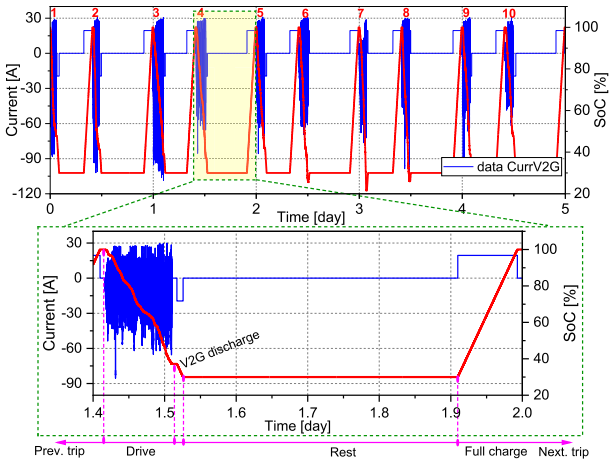

FIGURE 23. Intensive SoC operational profile with SC V2G strategy.

TABLE 10. Battery ageing results with SC V2G strategy for the first five-day operation.

Strategy	Profile	Rest time (h)	No. of Cycles	Calendar (%)	Cycle (%)	Total (%)
SC V2G	Gentle	81.3	7.1	0.0023	0.0117	0.0140
	Intensive	78.8	7.7	0.0025	0.0140	0.0165

to 91.5% and 25% increase for the gentle and intensive profiles, respectively. However, the total capacity loss under the gentle driving profile is reduced up to 28.7% while that of the intensive profile increases to 13.3% for the first five days operation when comparing to the SC V1G strategy. Notwithstanding, SC V2G strategy can mitigate a total ageing of 28.7% and 19.9% in the gentle and intensive profiles, respectively when comparing to the baseline STD CHA strategy. The results indicate that the SC V2G strategy can provide some benefits in both driving profiles as comparing to those of the baseline STD CHA approach.

E. SC VxG STRATEGY

It is noteworthy that the SC V1G strategy can reduce the calendar ageing by allowing the battery to be charged to the local optimal SoC, then leave the battery resting if the arrival SoC is smaller than the optimal SoC at a certain time. This charging strategy maintains the same resting duration and charge throughput compared to the conventional STD CHA and TS CHA approaches. Although there is no improvement in cycling ageing, the calendar ageing is still significantly reduced whenever the arrival SoC is smaller than the local optimal. Otherwise, the calendar ageing is somewhat diminished, especially when the arrival SoC is still high (i.e., for the gentle driving profile). Hence, this approach is not always the right choice since the arrival SoC of the real-world daily driving profile is usually unknown and varied depending on driver requirements.

SC V2G strategy overcomes the SC V1G drawback by allowing the battery to exchange their energy with the grid whenever the arrival SoC is different from the global

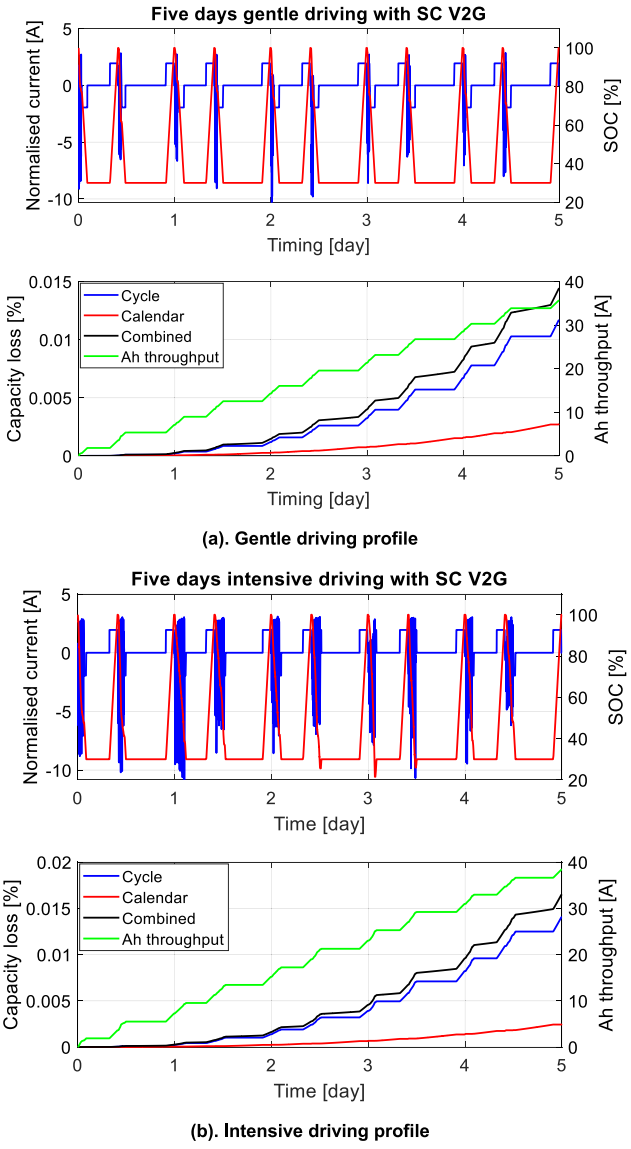

FIGURE 24. Prediction of battery ageing using SC V2G.

optimal SoC. Therefore, the battery can always rest at the global optimal SoC at any cases. This means that the calendar ageing can be remarkably improved by both reducing the resting time and turning the batteries to a global optimal SoC. However, although SC V2G can show benefits in both gentle and intensive driving profiles, this charging strategy causes the increment of charge throughput in general due to having extra charge and discharge cycles to bring the battery to an optimal SoC. Consequently, this potentially accelerates the battery cycling ageing in long-term operation, especially when the battery degrades.

To overcome the drawback of SC V1G and SC V2G, the SC VxG is developed as the combination of SC V1G and SC V2G methods to trade-off between the absolute difference of calendar ageing due to resting at optimal SoC and the absolute difference of cycling ageing due to having an addition of charge throughput (via bi-directional charging around

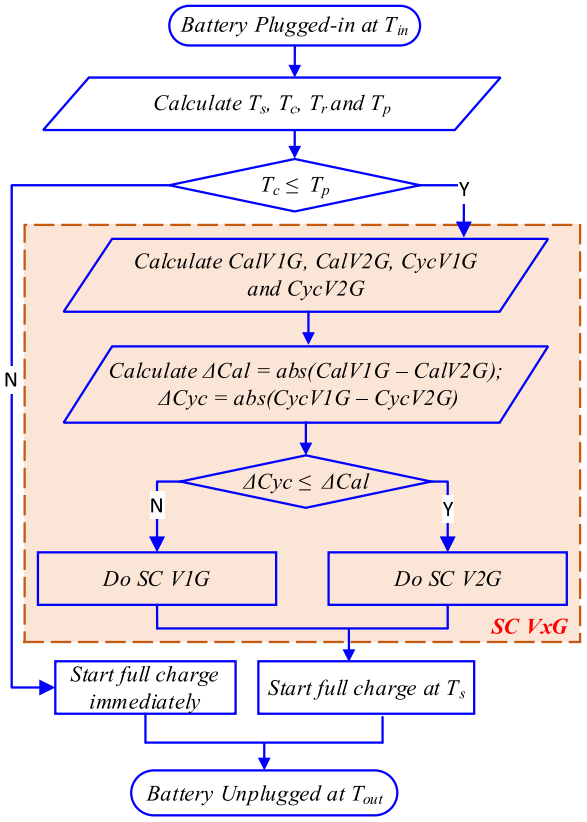

FIGURE 25. Combined smart charge pre-conditioning using SC VxG.

the optimal SoC). The combined model allows such two charging strategies to be switched back and forth, resulting in a reduction of the total ageing. Upon the parking of each trip and the battery is plugged-in, the controller determines whether it should go with either SC V1G or SC V2G. The arrival SoC and the current degradation status (or SoH) of the battery allows the controller to approximately estimate the total ageing of the battery in advance. Hence, the battery can only be participated in SC V2G if the absolute amount of cycling capacity loss is smaller than the those of calendar capacity loss at an instant of time, otherwise, the battery will be taken part in SC V1G.

A diagram of SC VxG approach is shown in Figure 25. *CalV1G* and *CycV1G* are the amount of calendar and cycling ageing when doing SC V1G. Similarly, *CalV2G* and *CycV2G* are the amount of calendar and cycling ageing when doing SC V2G. $\Delta Cal = abs\,(CalV1G -- CalV2G)$ is the absolute change of the calendar ageing between SC V1G and SC V2G. Likewise, $\Delta Cyc = abs\,(CycV1G -- CycV2G)$ is the absolute difference of the cycling ageing between the two methods. By considering the trade-off between ΔCal and ΔCyc, the SC VxG controller selects appropriate charging control method for each parking period.

Likewise, the top subplots in Figure 26 (a) and (b) depict the charging current and SoC variation profiles over time while the bottom subplots depict the predicted calendar and cycling capacity losses when using SC VxG strategy for the two mentioned driver profiles. Table 11 summarises the

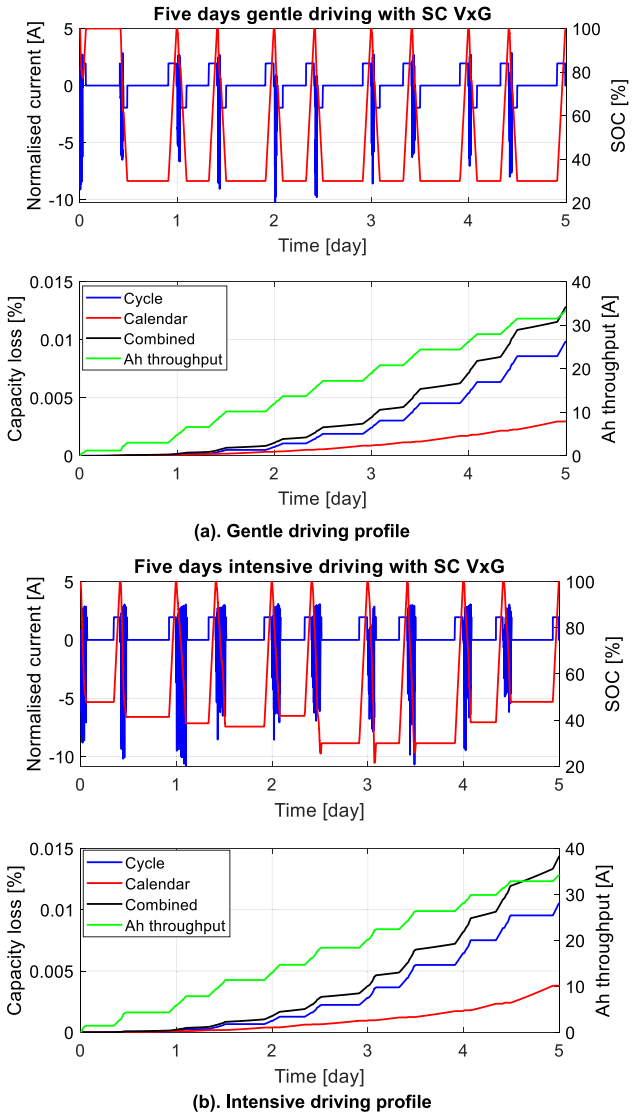

FIGURE 26. Prediction of battery ageing using SC VxG.

TABLE 11. Battery ageing results with SC VxG strategy for the first five-day operation.

Strategy	Profile	Rest time (h)	No. of Cycles	Calendar (%)	Cycle (%)	Total (%)
SC VxG	Gentle	83.9	6.7	0.0030	0.0098	0.0128
	Intensive	83.6	6.8	0.0039	0.0105	0.0144

battery ageing using SC VxG for the first five days operation. The SC VxG with the capability to balance the performance of SC V1G and SC V2G, it helps to improve the battery life significantly in most of the cases. Comparing to the baseline strategy, the calendar ageing is impressively diminished from 0.0185% to 0.003%, which is equivalent to 84% in the gentle profile, and from 0.0101% to 0.0039%, which is equivalent to 61% in the intensive profile. Although the cycling aging is increased due to having more charge throughput to reach the optimal SoC point, this reduction resulting the overall battery ageing is significantly reduced up to 34.4% and 30.1%

TABLE 12. Predicted capacity loss of different charging strategies.

No.	Days	Strategy	Gentle driving profile				Intensive driving profile			
			Calendar (%)	Cycle (%)	Total (%)	Mitigated (%)	Calendar (%)	Cycle (%)	Total (%)	Mitigated (%)
1	5	STD CHA	0.0185	0.001	0.0195	Baseline	0.0101	0.0105	0.0206	Baseline
		TS CHA	0.0191	0.001	0.0201	-3.1	0.0039	0.0105	0.0144	30.1
		SC V1G	0.0185	0.001	0.0195	0	0.0039	0.0105	0.0144	30.1
		SC V2G	0.0023	0.0117	0.0139	28.7	0.0025	0.014	0.0165	19.9
		SC VxG	0.003	0.0098	0.0128	34.4	0.0039	0.0105	0.0144	30.1
2	30	STD CHA	1.6331	0.0922	1.7253	Baseline	0.8863	0.9002	1.7865	Baseline
		TS CHA	1.6769	0.0922	1.7691	-2.5	0.3448	0.9002	1.245	30.3
		SC V1G	1.6022	0.0922	1.6944	1.8	0.3396	0.9002	1.2398	30.6
		SC V2G	0.2438	0.9522	1.196	30.7	0.2174	1.0548	1.2722	28.8
		SC VxG	0.2472	0.938	1.1852	31.3	0.3396	0.9002	1.2398	30.6
3	100	STD CHA	2.8339	1.3373	4.1712	Baseline	2.5986	3.0781	5.6767	Baseline
		TS CHA	2.9558	1.3373	4.2931	-2.9	1.0238	3.078	4.1018	27.7
		SC V1G	2.7629	1.3373	4.1002	1.7	1.0098	3.0783	4.0881	28
		SC V2G	0.794	3.1996	3.9936	4.3	0.7538	3.4349	4.1887	26.2
		SC VxG	1.1336	2.7327	3.8663	7.3	0.9778	3.181	4.1588	26.7
4	365	STD CHA	4.1991	4.4211	8.6202	Baseline	3.6351	7.918	11.5531	Baseline
		TS CHA	4.7066	4.4211	9.1277	-5.9	1.9093	7.9181	9.8274	14.9
		SC V1G	4.1675	4.4211	8.5886	0.4	1.9093	7.9178	9.8271	14.9
		SC V2G	1.4875	8.5157	10.0032	-16	1.4789	8.8459	10.3248	10.6
		SC VxG	2.5816	5.2958	7.8774	8.6	1.8004	8.3284	10.1288	12.3

for the gentle and intensive driving profiles, respectively. Therefore, by taking advantages of both SC V1G and SC V2G strategies, the proposed SC VxG strategy can minimise the total degradation at any instant during the whole life of the battery. It is suitable for long-term prediction, especially when the battery is aged.

F. DISCUSSIONS

From the above results and analysis, all charging approaches can reduce the total battery ageing as comparing to the base line STD CHA method for the intensive driving profile. The total battery ageing can be mitigated by reducing either calendar ageing or charge throughput. Particularly, both the TS CHA and SC V1G strategies show crucial benefits as they significantly demonstrate the improvement in battery degradation (up to 30%). The SC V2G adds more capability to the SC V1G, but it also increases the charge throughput, hence the total ageing is increased in some cases. The combined SC VxG gains the advantages of both the SC V1G and SC V2G so that it can designate suitable charging strategy at any period. It allows the charger to interchange between the two strategies according to the current degradation status of the battery. Hence, the total ageing mitigation is ensured to be between those of the SC V1G and SC V2G.

A dynamic pre-conditioning strategy is required to adapt to different battery conditions and driving styles of drivers. For instance, the performance of charging strategies is considerably varied for the gentle driving profile. The TS CHA and SC V1G are not suitable for this kind of driving style because they have very minor improvement on battery degradation or even increase it in some cases compared to the baseline STD CHA. In contrast, the SC V2G shows benefits in this case since the reducing of calendar ageing is more outstanding than the increment of cycling ageing. However, it is not feasible for a degraded battery as the cycling aging rate is high. The combined SC VxG strategy once again demonstrates the helpfulness by dynamically switching between SC V1G and SC V2G to reach the optimal operational condition, subsequently minimising the total battery degradation.

It is noteworthy that for calendar aging, the capacity loss prediction is dependent on battery SoH. The storing time is one major dependency of the calendar aging model, which is accumulated from all separate resting periods during the whole life. Likewise, for the cycling ageing, the total charge throughput is one critical element which affects the estimation of cycling capacity fade. The developed degradation models establish the ability to evaluate degradation performance of the battery using various charging strategies under various driving styles. These models are fully applicable to be employed to evaluate the complete degradation behaviours of the battery in long time usage.

To better understand the ageing behaviours of the battery with respect to the five charging strategies for long-term operational conditions, each charging approach is applied

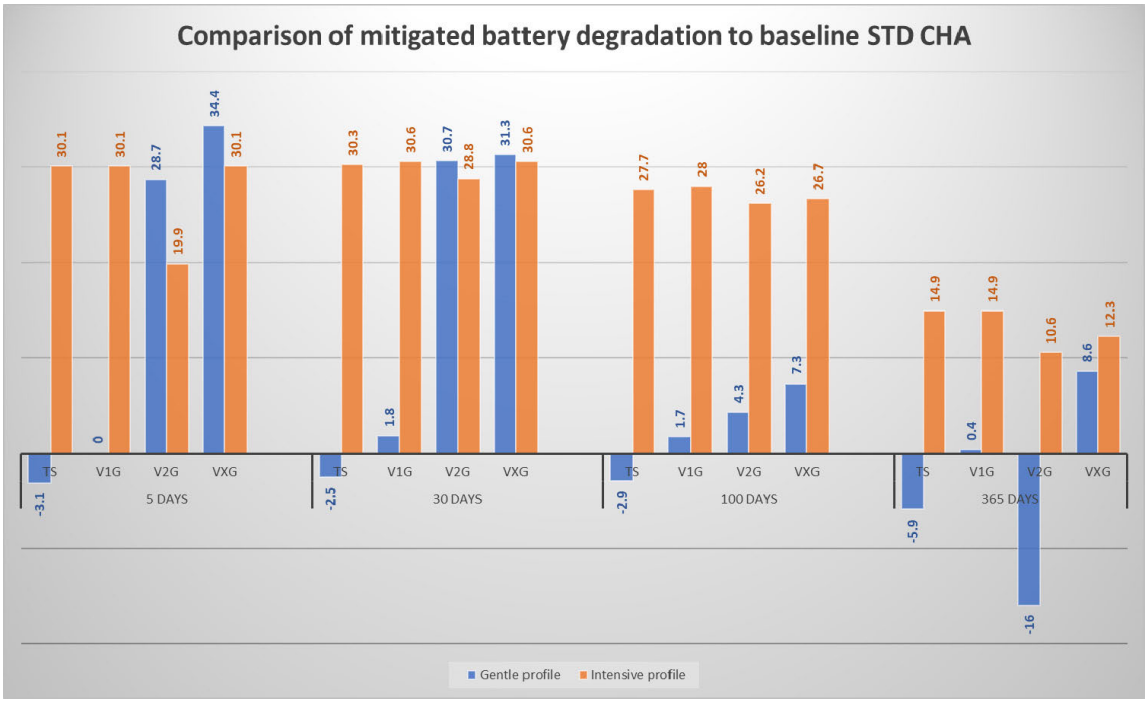

FIGURE 27. Comparison of reduced battery degradation through different charging strategies.

continuously for 365 days via extended simulation. Table 12 summarizes the predicted capacity losses of the comparative charging strategies for 365 days of operation. Here, the "Mitigated" columns present the reduced percentage of the total degradation of each approach as comparing to the baseline STD CHA, in which positive values indicate the positive impacts of changing strategies on the improvement of battery ageing (mitigated battery capacity fade) and vice versa.

From this table, the performance of the TS CHA and SC V1G in mitigating the total battery degradation is varied between the gentle and intensive driving profiles. This behaviour demonstrates the impacts of the arrival SoC and local optimal SoC on the value degradation experienced by the battery. For a 365-day operation, the mitigation of battery degradation employing these strategies are significant with respect to the intensive profile (both mitigating up to 14.9% of battery ageing). However, this improvement is insignificant with the gentle profile (−5.9% and 0.4% for the cases using TS CHA and SC V1G compared to the baseline, respectively). The SC V2G and SC VxG strategies always demonstrate their effectiveness in reducing the battery degradation. The SC V2G can improve the battery ageing up to 10.6% in the intensive profile since it always allows the battery to be at rest at the global optimal SoC.

Although SC V2G functions well when the battery is relatively new, its performance deteriorates when the battery degrades under the gentle profile (negatively impacting the degradation by −16% after 365 days operation). This is because the global optimal SoC changes over time and it requires more charge throughput as the consequence of bi-directional charging. It is notable that the degradation improvement utilising the SC V2G will be more significant if the updated global optimal SoC is higher than the arrival SoC. This behaviour once again highlights the impact of the arrival SoC to the performance of each charging strategy. A similar trend can be seen with the SC VxG. However, due to its unique capability of dynamically switching back and forth between SC V1G and SC V2G to select an optimal strategy, SC VxG always shows the benefits in mitigating the battery degradation for both driving profiles. Figure 27 highlights the comparison of different charging strategies to their baseline STD CHA strategy. From the results, it can be seen that all the pre-conditioning strategies improved battery life when operating with gentle driver profile, having higher starting SoC. However, there was the possibility of the SC V2G to further degrade the battery faster due to increased charge throughput (increased 16% of capacity loss after one year of operational life). The TS CHA increased degradation due to particularity within this cell formulation (added 5.6% of ageing). The SC VxG strategy continued to improve battery life because it balances both ageing of the SC V1G and SC V2G (reduced 8.6% of battery degradation after one year operating comparing to the baseline STD CHA). For the intensive driver profile, all pre-conditioning strategies improved battery life significantly (10.6 – 14.9%). The TS CHA provided the most gain (14.9%) for this cell type with least complexity. SC V1G and SC V2G strategies demonstrated the advantages in reducing the ageing rate of the battery while the SC VxG strategy demonstrated its capability in balancing the performance of SC V1G and SC V2G to achieve the best accomplishment. However, after long-term usage or as the battery

degrades, the increased charge throughput to condition the battery started to accelerate degradation.

It is noteworthy that beside the mitigation in term of total capacity loss, the SC V2G and SC VxG can export some amount of energy from the battery to support the electrical grid or energy storage. Hence, some revenue can be earned if there is an appropriate usage of such energy. Therefore, a future optimisation strategy is necessary to select suitable charging approaches at an instant of time and/or actual battery SoH so that it can optimise the battery degradation during the whole life of the battery.

IV. CONCLUSION AND FUTURE WORKS

A. CONCLUSION

In this paper, semi-empirical degradation models were developed and validated for calendar and cycling ageing based on historical ageing datasets to predict the degradation of an EV battery. A combined ageing model was developed by combining the validated calendar and cycling ageing models to predict the total ageing behaviour of the battery under five different SoC pre-conditioning strategies for V2G applications. Two driving profiles representing the gentle and intensive energy drivers were introduced to evaluate the performance of such charging approaches. Each charging strategy illustrated the relative advantage and disadvantages in minimizing the battery degradation due to calendar and cycling ageing during the parking period of the EV. Simulation of the battery ageing under five charging strategies were performed. The results were compared and analysed to facilitate forecasting of the impact of the battery degradation on pre-V2G operation scenarios. The proposed charging strategies could mitigate the total ageing of the employed battery from 8.6 – 12.3% for one-year continual operation compared to the reference standard charging approach.

The TS CHA and SC V1G strategies perform consistently well in reducing the battery ageing under the intensive driving profile while they create negative impact on the battery degradation under the gentle driving profile. The SC V2G and SC VxG strategies mitigate the battery ageing in most cases, especially when the battery is new. However, their capability will be reduced along with the battery SoH reduction, at which the decrement of calendar capacity loss does not supersede the increment of cycling ageing. The charging performance of these approaches is also significantly affected by the variations of local and global optimal SoCs.

B. FUTURE WORKS

Five primary elements of further works remain are:

- First, complete validation of the degradation models with extended ageing data is required to fully verify the applicability of the developed models under different operating conditions. Particularly, for the cycling ageing model with increased operational temperatures and the combined model with mixed calendar and cycling or with real-life drive cycles.
- Second, to better support the evaluation of the degradation models, a comparison can be made between the model presented here and different methods of ageing model construction, such as fully empirical models or physics-based models. This will require the formulation of appropriate datasets to allow model parameterization in each case. The potential value would be the ability to easily evaluate predictions of battery life without the need to undertake extensive ageing experiments. In addition, the ability to corelate battery ageing with those forms of model that provide a greater insight into the mechanisms of ageing, may also highlight the nature of the underpinning causes of degradation.
- Third, the developed models can be employed to evaluate the battery degradation with actual V2G scenarios (such as frequency regulation, peak shaving and load levelling). These tasks can be conducted when the battery is in resting mode, after the SoC pre-conditioning process. Hence, true V2G scenarios on top of SoC pre-conditioning require an advanced optimal algorithm including the definition of a cost function, in which the value of the optimisation problem is based on electrical price and battery degradation, to control the charge and discharge rates so that either maximising the revenue or minimising the total battery degradation.
- Fourth, additional research on the influence of ambient temperature on the ageing behaviour should be considered. This requires the construction of a more diverse dataset in which a wider range of ambient temperatures are investigated for both calendar and cyclic ageing. From this data, the ageing models can be retrained and validated, thereby improving their ability to accurately represent battery operation and ageing in the real-world.
- Finally, the degradation of the battery is expected to vary in line with changes in form factor and chemistry. Further research is therefore required to understand the transferability of the methodology. The authors acknowledge that the model will most likely require recalibration for use with other technologies, that will in turn require additional training datasets to be produced. However, the authors assert that the underpinning techniques for parameterization and model structure will be transferable and scalable as the model is transitioned from cell-level studies through to system and vehicle-level research.

REFERENCES

[1] M. Petit, E. Prada, and V. Sauvant-Moynot, "Development of an empirical aging model for Li-ion batteries and application to assess the impact of vehicle-to-grid strategies on battery lifetime," *Appl. Energy*, vol. 172, pp. 398–407, Jun. 2016, doi: 10.1016/j.apenergy.2016.03.119.

[2] A. Ahmadian, M. Sedghi, B. Mohammadi-Ivatloo, A. Elkamel, M. A. Golkar, and M. Fowler, "Cost-benefit analysis of V2G implementation in distribution networks considering PEVs battery degradation," *IEEE Trans. Sustain. Energy*, vol. 9, no. 2, pp. 961–970, Apr. 2018, doi: 10.1109/TSTE.2017.2768437.

[3] Y. Zheng, S. Niu, Y. Shang, Z. Shao, and L. Jian, "Integrating plug-in electric vehicles into power grids: A comprehensive review on power interaction mode, scheduling methodology and mathematical foundation," *Renew. Sustain. Energy Rev.*, vol. 112, pp. 424–439, Sep. 2019, doi: 10.1016/j.rser.2019.05.059.

[4] O. Kolawole and I. Al-Anbagi, "Electric vehicles battery wear cost optimization for frequency regulation support," *IEEE Access*, vol. 7, pp. 130388–130398, 2019, doi: 10.1109/ACCESS.2019.2930233.

[5] K. M. Rogers, R. Klump, H. Khurana, A. A. Aquino-Lugo, and T. J. Overbye, "An authenticated control framework for distributed voltage support on the smart grid," *IEEE Trans. Smart Grid*, vol. 1, no. 1, pp. 40–47, Jun. 2010, doi: 10.1109/TSG.2010.2044816.

[6] M. Soltani, J. Ronsmans, and J. Van Mierlo, "Cycle life and calendar life model for lithium-ion capacitor technology in a wide temperature range," *J. Energy Storage*, vol. 31, Oct. 2020, Art. no. 101659, doi: 10.1016/j.est.2020.101659.

[7] X. Han, L. Lu, Y. Zheng, X. Feng, Z. Li, J. Li, and M. Ouyang, "A review on the key issues of the lithium ion battery degradation among the whole life cycle," *eTransportation*, vol. 1, Aug. 2019, Art. no. 100005, doi: 10.1016/j.etran.2019.100005.

[8] J. Guo, J. Yang, Z. Lin, C. Serrano, and A. M. Cortes, "Impact analysis of V2G services on EV battery degradation—A review," in *Proc. IEEE Milan PowerTech.*, Jun. 2019, pp. 1–6, doi: 10.1109/PTC.2019.8810982.

[9] A. J. Smith, H. M. Dahn, J. C. Burns, and J. R. Dahn, "Long-term low-rate cycling of $LiCoO_2$/graphite Li-ion cells at 55°C," *J. Electrochem. Soc.*, vol. 159, no. 6, pp. A705–A710, 2012, doi: 10.1149/2.056206jes.

[10] P. Keil, S. F. Schuster, J. Wilhelm, J. Travi, A. Hauser, R. C. Karl, and A. Jossen, "Calendar aging of lithium-ion batteries," *J. Electrochem. Soc.*, vol. 163, no. 9, pp. A1872–A1880, 2016, doi: 10.1149/2.0411609jes.

[11] K. Liu, T. R. Ashwin, X. Hu, M. Lucu, and W. D. Widanage, "An evaluation study of different modelling techniques for calendar ageing prediction of lithium-ion batteries," *Renew. Sustain. Energy Rev.*, vol. 131, Oct. 2020, Art. no. 110017, doi: 10.1016/j.rser.2020.110017.

[12] H. Farzin, M. Fotuhi-Firuzabad, and M. Moeini-Aghtaie, "A practical scheme to involve degradation cost of lithium-ion batteries in vehicle-to-grid applications," *IEEE Trans. Sustain. Energy*, vol. 7, no. 4, pp. 1730–1738, Oct. 2016, doi: 10.1109/TSTE.2016.2558500.

[13] K. Ginigeme and Z. Wang, "Distributed optimal vehicle-to-grid approaches with consideration of battery degradation cost under real-time pricing," *IEEE Access*, vol. 8, pp. 5225–5235, 2020, doi: 10.1109/ACCESS.2019.2963692.

[14] S.-A. Amamra and J. Marco, "Vehicle-to-grid aggregator to support power grid and reduce electric vehicle charging cost," *IEEE Access*, vol. 7, pp. 178528–178538, 2019, doi: 10.1109/ACCESS.2019.2958664.

[15] K. Uddin, M. Dubarry, and M. B. Glick, "The viability of vehicle-to-grid operations from a battery technology and policy perspective," *Energy Policy*, vol. 113, pp. 342–347, Feb. 2018, doi: 10.1016/j.enpol.2017.11.015.

[16] Y. Yu, O. S. Nduka, and B. C. Pal, "Smart control of an electric vehicle for ancillary service in DC microgrid," *IEEE Access*, vol. 8, pp. 197222–197235, 2020, doi: 10.1109/ACCESS.2020.3034496.

[17] A. Marongiu, M. Roscher, and D. U. Sauer, "Influence of the vehicle-to-grid strategy on the aging behavior of lithium battery electric vehicles," *Appl. Energy*, vol. 137, pp. 899–912, Jan. 2015, doi: 10.1016/j.apenergy.2014.06.063.

[18] J. de Hoog, "Combined cycling and calendar capacity fade modeling of a Nickel-manganese-cobalt oxide cell with real-life profile validation," *Appl. Energy*, vol. 200, pp. 47–61, Aug. 2017, doi: 10.1016/j.apenergy.2017.05.018.

[19] E. Redondo-Iglesias, P. Venet, and S. Pelissier, "Modelling lithium-ion battery ageing in electric vehicle applications—Calendar and cycling ageing combination effects," *Batteries*, vol. 6, no. 1, p. 14, Feb. 2020, doi: 10.3390/batteries6010014.

[20] G. Zhang, S. T. Tan, and G. G. Wang, "Real-time smart charging of electric vehicles for demand charge reduction at non-residential sites," *IEEE Trans. Smart Grid*, vol. 9, no. 5, pp. 4027–4037, Sep. 2018, doi: 10.1109/TSG.2016.2647620.

[21] N. I. Nimalsiri, C. P. Mediwaththe, E. L. Ratnam, M. Shaw, D. B. Smith, and S. K. Halgamuge, "A survey of algorithms for distributed charging control of electric vehicles in smart grid," *IEEE Trans. Intell. Transp. Syst.*, vol. 21, no. 11, pp. 4497–4515, Nov. 2019, doi: 10.1109/TITS.2019.2943620.

[22] J. D. K. Bishop, C. J. Axon, D. Bonilla, M. Tran, D. Banister, and M. D. McCulloch, "Evaluating the impact of V2G services on the degradation of batteries in PHEV and EV," *Appl. Energy*, vol. 111, pp. 206–218, Nov. 2013, doi: 10.1016/j.apenergy.2013.04.094.

[23] C. Zhou, K. Qian, M. Allan, and W. Zhou, "Modeling of the cost of EV battery wear due to V2G application in power systems," *IEEE Trans. Energy Convers.*, vol. 26, no. 4, pp. 1041–1050, Dec. 2011, doi: 10.1109/TEC.2011.2159977.

[24] C. Guenther, B. Schott, W. Hennings, P. Waldowski, and M. A. Danzer, "Model-based investigation of electric vehicle battery aging by means of vehicle-to-grid scenario simulations," *J. Power Sources*, vol. 239, pp. 604–610, Oct. 2013, doi: 10.1016/j.jpowsour.2013.02.041.

[25] M. Nour, S. M. Said, A. Ali, and C. Farkas, "Smart charging of electric vehicles according to electricity price," in *Proc. Int. Conf. Innov. Trends Comput. Eng. (ITCE)*, Feb. 2019, pp. 432–437, doi: 10.1109/ITCE.2019.8646425.

[26] D. T. Hoang, P. Wang, D. Niyato, and E. Hossain, "Charging and discharging of plug-in electric vehicles (PEVs) in vehicle-to-grid (V2G) systems: A cyber insurance-based model," *IEEE Access*, vol. 5, pp. 732–754, 2017, doi: 10.1109/ACCESS.2017.2649042.

[27] A. Ahmadian, M. Sedghi, A. Elkamel, M. Fowler, and M. A. Golkar, "Plug-in electric vehicle batteries degradation modeling for smart grid studies: Review, assessment and conceptual framework," *Renew. Sustain. Energy Rev.*, vol. 81, pp. 2609–2624, Jan. 2017, doi: 10.1016/j.rser.2017.06.067.

[28] Y. Wang and Z. Chen, "A framework for state-of-charge and remaining discharge time prediction using unscented particle filter," *Appl. Energy*, vol. 260, Feb. 2020, Art. no. 114324, doi: 10.1016/j.apenergy.2019.114324.

[29] Y. Wang, J. Tian, Z. Sun, L. Wang, R. Xu, M. Li, and Z. Chen, "A comprehensive review of battery modeling and state estimation approaches for advanced battery management systems," *Renew. Sustain. Energy Rev.*, vol. 131, Oct. 2020, Art. no. 110015, doi: 10.1016/j.rser.2020.110015.

[30] M. Lucu, E. Martinez-Laserna, I. Gandiaga, K. Liu, H. Camblong, W. D. Widanage, and J. Marco, "Data-driven nonparametric li-ion battery ageing model aiming at learning from real operation data—Part B: Cycling operation," *J. Energy Storage*, vol. 30, Aug. 2020, Art. no. 101410, doi: 10.1016/j.est.2020.101410.

[31] X. Jin, A. Vora, V. Hoshing, T. Saha, G. Shaver, O. Wasynczuk, and S. Varigonda, "Applicability of available li-ion battery degradation models for system and control algorithm design," *Control Eng. Pract.*, vol. 71, pp. 1–9, Feb. 2018, doi: 10.1016/j.conengprac.2017.10.002.

[32] M. Naumann, M. Schimpe, P. Keil, H. C. Hesse, and A. Jossen, "Analysis and modeling of calendar aging of a commercial $LiFePO_4$/graphite cell," *J. Energy Storage*, vol. 17, pp. 153–169, Jun. 2018, doi: 10.1016/j.est.2018.01.019.

[33] M. Naumann, F. B. Spingler, and A. Jossen, "Analysis and modeling of cycle aging of a commercial $LiFePO_4$/graphite cell," *J. Power Sources*, vol. 451, Mar. 2020, Art. no. 227666, doi: 10.1016/j.jpowsour.2019.227666.

[34] Y. Li, K. Li, Y. Xie, J. Liu, C. Fu, and B. Liu, "Optimized charging of lithium-ion battery for electric vehicles: Adaptive multistage constant current–constant voltage charging strategy," *Renew. Energy*, vol. 146, pp. 2688–2699, Feb. 2020, doi: 10.1016/j.renene.2019.08.077.

[35] J. Wu, Z. Wei, K. Liu, Z. Quan, and Y. Li, "Battery-involved energy management for hybrid electric bus based on expert-assistance deep deterministic policy gradient algorithm," *IEEE Trans. Veh. Technol.*, vol. 69, no. 11, pp. 12786–12796, Nov. 2020, doi: 10.1109/TVT.2020.3025627.

[36] J. Wu, Z. Wei, W. Li, Y. Wang, Y. Li, and D. U. Sauer, "Battery Thermal- and health-constrained energy management for hybrid electric bus based on soft actor-critic DRL algorithm," *IEEE Trans. Ind. Informat.*, vol. 17, no. 6, pp. 3751–3761, Jun. 2021, doi: 10.1109/TII.2020.3014599.

[37] Y. Wang, G. Gao, X. Li, and Z. Chen, "A fractional-order model-based state estimation approach for lithium-ion battery and ultracapacitor hybrid power source system considering load trajectory," *J. Power Sources*, vol. 449, Feb. 2020, Art. no. 227543, doi: 10.1016/j.jpowsour.2019.227543.

[38] A. Barré, B. Deguilhem, S. Grolleau, M. Gérard, F. Suard, and D. Riu, "A review on lithium-ion battery ageing mechanisms and estimations for automotive applications," *J. Power Sources*, vol. 241, pp. 680–689, Nov. 2013, doi: 10.1016/j.jpowsour.2013.05.040.

[39] Y. Li, M. Vilathgamuwa, S. S. Choi, B. Xiong, J. Tang, Y. Su, and Y. Wang, "Design of minimum cost degradation-conscious lithium-ion battery energy storage system to achieve renewable power dispatchability," *Appl. Energy*, vol. 260, Feb. 2020, Art. no. 114282, doi: 10.1016/j.apenergy.2019.114282.
[40] C. Li, N. Cui, C. Wang, and C. Zhang, "Reduced-order electrochemical model for lithium-ion battery with domain decomposition and polynomial approximation methods," *Energy*, vol. 221, Apr. 2021, Art. no. 119662, doi: 10.1016/j.energy.2020.119662.
[41] X. Zhang, Y. Gao, B. Guo, C. Zhu, X. Zhou, L. Wang, and J. Cao, "A novel quantitative electrochemical aging model considering side reactions for lithium-ion batteries," *Electrochimica Acta*, vol. 343, May 2020, Art. no. 136070, doi: 10.1016/j.electacta.2020.136070.
[42] Y. Li, K. Liu, A. M. Foley, A. Zálke, M. Berecibar, E. Nanini-Maury, J. Van Mierlo, and H. E. Hoster, "Data-driven health estimation and lifetime prediction of lithium-ion batteries: A review," *Renew. Sustain. Energy Rev.*, vol. 113, Oct. 2019, Art. no. 109254, doi: 10.1016/j.rser.2019.109254.
[43] M. Lucu, E. Martinez-Laserna, I. Gandiaga, and H. Camblong, "A critical review on self-adaptive Li-ion battery ageing models," *J. Power Sources*, vol. 401, pp. 85–101, Oct. 2018, doi: 10.1016/j.jpowsour.2018.08.064.
[44] C. Lin, A. Tang, and W. Wang, "A review of SOH estimation methods in lithium-ion batteries for electric vehicle applications," *Energy Proc.*, vol. 75, pp. 1920–1925, Aug. 2015, doi: 10.1016/j.egypro.2015.07.199.
[45] Y. Jiang, J. Zhang, L. Xia, and Y. Liu, "State of health estimation for lithium-ion battery using empirical degradation and error compensation models," *IEEE Access*, vol. 8, pp. 123858–123868, 2020, doi: 10.1109/ACCESS.2020.3005229.
[46] G. Saldana, J. I. S. Martin, I. Zamora, F. J. Asensio, O. Onederra, and M. Gonzalez, "Empirical electrical and degradation model for electric vehicle batteries," *IEEE Access*, vol. 8, pp. 155576–155589, 2020, doi: 10.1109/ACCESS.2020.3019477.
[47] M. Varini, P. E. Campana, and G. Lindbergh, "A semi-empirical, electrochemistry-based model for li-ion battery performance prediction over lifetime," *J. Energy Storage*, vol. 25, Oct. 2019, Art. no. 100819, doi: 10.1016/j.est.2019.100819.
[48] Z. Wei, Z. Quan, J. Wu, Y. Li, J. Pou, and H. Zhong, "Deep deterministic policy gradient-DRL enabled multiphysics-constrained fast charging of lithium-ion battery," *IEEE Trans. Ind. Electron.*, early access, Apr. 7, 2021 doi: 10.1109/TIE.2021.3070514.
[49] A. Barai, G. H. Chouchelamane, Y. Guo, A. McGordon, and P. Jennings, "A study on the impact of lithium-ion cell relaxation on electrochemical impedance spectroscopy," *J. Power Sources*, vol. 280, pp. 74–80, Apr. 2015, doi: 10.1016/j.jpowsour.2015.01.097.
[50] J. Marco, N. Kumari, W. Widanage, and P. Jones, "A cell-in-the-loop approach to systems modelling and simulation of energy storage systems," *Energies*, vol. 8, no. 8, pp. 8244–8262, Aug. 2015, doi: 10.3390/en8088244.
[51] M. F. Niri, T. M. N. Bui, T. Q. Dinh, E. Hosseinzadeh, T. F. Yu, and J. Marco, "Remaining energy estimation for lithium-ion batteries via Gaussian mixture and Markov models for future load prediction," *J. Energy Storage*, vol. 28, Apr. 2020, Art. no. 101271, doi: 10.1016/j.est.2020.101271.
[52] A. Barai, K. Uddin, M. Dubarry, L. Somerville, A. McGordon, P. Jennings, and I. Bloom, "A comparison of methodologies for the non-invasive characterisation of commercial li-ion cells," *Prog. Energy Combustion Sci.*, vol. 72, pp. 1–31, May 2019, doi: 10.1016/j.pecs.2019.01.001.
[53] M. Dubarry and G. Baure, "Perspective on commercial li-ion battery testing, best practices for simple and effective protocols," *Electronics*, vol. 9, no. 1, p. 152, Jan. 2020, doi: 10.3390/electronics9010152.
[54] E. Sarasketa-Zabala, I. Gandiaga, E. Martinez-Laserna, L. M. Rodriguez-Martinez, and I. Villarreal, "Cycle ageing analysis of a $LiFePO_4$/graphite cell with dynamic model validations: Towards realistic lifetime predictions," *J. Power Sources*, vol. 275, pp. 573–587, Feb. 2015, doi: 10.1016/j.jpowsour.2014.10.153.
[55] E. Redondo-Iglesias, P. Venet, and S. Pelissier, "Calendar and cycling ageing combination of batteries in electric vehicles," *Microelectron. Rel.*, vol.s. 88–90, pp. 1212–1215, Sep. 2018, doi: 10.1016/j.microrel.2018.06.113.
[56] E. Sarasketa-Zabala, E. Martinez-Laserna, M. Berecibar, I. Gandiaga, L. M. Rodriguez-Martinez, and I. Villarreal, "Realistic lifetime prediction approach for Li-ion batteries," *Appl. Energy*, vol. 162, pp. 839–852, Jan. 2016, doi: 10.1016/j.apenergy.2015.10.115.
[57] K. Liu, Y. Li, X. Hu, M. Lucu, and W. D. Widanage, "Gaussian process regression with automatic relevance determination kernel for calendar aging prediction of lithium-ion batteries," *IEEE Trans. Ind. Informat.*, vol. 16, no. 6, pp. 3767–3777, Jun. 2020, doi: 10.1109/TII.2019.2941747.

TRUONG M. N. BUI received the Ph.D. degree in mechatronics from the University of Ulsan, South Korea. He is currently a Research Fellow with the Warwick Manufacturing Group (WMG), University of Warwick, Coventry, U.K. His research interests include control applications, energy storage system modeling, energy and battery management systems, V2G applications, and real-time control for EV/HEVs applications.

MUHAMMAD SHEIKH received the Ph.D. degree from the University of Sunderland, U.K. He worked as a Research Associate. He is currently a Project Engineer with WMG, University of Warwick, U.K. His research interests include ageing and degradation studies of Lithium-ion batteries. He is also involved with academic and commercial projects for Li-ion cell behaviours under various operating conditions.

TRUONG Q. DINH (Senior Member, IEEE) received the Ph.D. degree (Hons.) in mechatronics from the University of Ulsan, South Korea. He is currently an Associate Professor with WMG, University of Warwick, U.K. His research interests include mechatronics, control theories and applications, modeling, management and control of energy systems, and advanced propulsion systems.

ANIRUDDHA GUPTA received the Ph.D. degree in engineering from the University of Warwick, Coventry, U.K. He is currently a Project Engineer with WMG, University of Warwick, on industrial projects in collaboration with Aston Martin, Jaguar Land Rover, and NHS. His research interests include the areas of implementation of big data analytics and machine learning techniques for automotive battery capacity fade prediction.

DHAMMIKA W. WIDANALAGE (Member, IEEE) received the Ph.D. degree in system identification from the University of Warwick, Coventry, U.K. He is currently an Associate Professor in modeling and energy storage at WMG, University of Warwick. His research interest includes system identification theory, applied across several applications, including batteries.

JAMES MARCO received the Eng.D. degree from the University of Warwick, Coventry, U.K. He is currently a Professor with WMG, University of Warwick. He is a Chartered Engineer and a fellow of the Institution of Engineering and Technology (IET). His research interests include battery systems engineering, real-time control, energy storage modeling and characterization, and smart battery development.